

KERNELIZED LEARNING METHODS IN AUTOMATIC CONTROL

THIS IS A TEMPORARY TITLE PAGE
It will be replaced for the final print by a version
provided by the registrar's office.

Thèse n. 1234 2022
présentée le 23 septembre 2022
à la Faculté des sciences de base
laboratoire SuperScience
programme doctoral en SuperScience
École polytechnique fédérale de Lausanne
pour l'obtention du grade de Docteur ès Sciences
par

Paolino Paperino

acceptée sur proposition du jury :

Prof Name Surname, président du jury
Prof Name Surname, directeur de thèse
Prof Name Surname, rapporteur
Prof Name Surname, rapporteur
Prof Name Surname, rapporteur

EPFL

Lausanne, EPFL, 2022

Besides this'll be easy with the two of us.

We've got science on our side.

— Bonnibel Bubblegum

Acknowledgment

put your text here

Bienne, September 23, 2022

Emilio Tanowe Maddalena

Abstract

Lorem ipsum dolor sit amet, consectetuer adipiscing elit. Ut purus elit, vestibulum ut, placerat ac, adipiscing vitae, felis. Curabitur dictum gravida mauris. Nam arcu libero, nonummy eget, consectetuer id, vulputate a, magna. Donec vehicula augue eu neque. Pellentesque habitant morbi tristique senectus et netus et malesuada fames ac turpis egestas. Mauris ut leo. Cras viverra metus rhoncus sem. Nulla et lectus vestibulum urna fringilla ultrices. Phasellus eu tellus sit amet tortor gravida placerat. Integer sapien est, iaculis in, pretium quis, viverra ac, nunc. Praesent eget sem vel leo ultrices bibendum. Aenean faucibus. Morbi dolor nulla, malesuada eu, pulvinar at, mollis ac, nulla. Curabitur auctor semper nulla. Donec varius orci eget risus. Duis nibh mi, congue eu, accumsan eleifend, sagittis quis, diam. Duis eget orci sit amet orci dignissim rutrum.

Nam dui ligula, fringilla a, euismod sodales, sollicitudin vel, wisi. Morbi auctor lorem non justo. Nam lacus libero, pretium at, lobortis vitae, ultricies et, tellus. Donec aliquet, tortor sed accumsan bibendum, erat ligula aliquet magna, vitae ornare odio metus a mi. Morbi ac orci et nisl hendrerit mollis. Suspendisse ut massa. Cras nec ante. Pellentesque a nulla. Cum sociis natoque penatibus et magnis dis parturient montes, nascetur ridiculus mus. Aliquam tincidunt urna. Nulla ullamcorper vestibulum turpis. Pellentesque cursus luctus mauris.

Zusammenfassung

Lorem ipsum dolor sit amet, consectetuer adipiscing elit. Ut purus elit, vestibulum ut, placerat ac, adipiscing vitae, felis. Curabitur dictum gravida mauris. Nam arcu libero, nonummy eget, consectetuer id, vulputate a, magna. Donec vehicula augue eu neque. Pellentesque habitant morbi tristique senectus et netus et malesuada fames ac turpis egestas. Mauris ut leo. Cras viverra metus rhoncus sem. Nulla et lectus vestibulum urna fringilla ultrices. Phasellus eu tellus sit amet tortor gravida placerat. Integer sapien est, iaculis in, pretium quis, viverra ac, nunc. Praesent eget sem vel leo ultrices bibendum. Aenean faucibus. Morbi dolor nulla, malesuada eu, pulvinar at, mollis ac, nulla. Curabitur auctor semper nulla. Donec varius orci eget risus. Duis nibh mi, congue eu, accumsan eleifend, sagittis quis, diam. Duis eget orci sit amet orci dignissim rutrum.

Nam dui ligula, fringilla a, euismod sodales, sollicitudin vel, wisi. Morbi auctor lorem non justo. Nam lacus libero, pretium at, lobortis vitae, ultricies et, tellus. Donec aliquet, tortor sed accumsan bibendum, erat ligula aliquet magna, vitae ornare odio metus a mi. Morbi ac orci et nisl hendrerit mollis. Suspendisse ut massa. Cras nec ante. Pellentesque a nulla. Cum sociis natoque penatibus et magnis dis parturient montes, nascetur ridiculus mus. Aliquam tincidunt urna. Nulla ullamcorper vestibulum turpis. Pellentesque cursus luctus mauris.

Résumé

Lorem ipsum dolor sit amet, consectetuer adipiscing elit. Ut purus elit, vestibulum ut, placerat ac, adipiscing vitae, felis. Curabitur dictum gravida mauris. Nam arcu libero, nonummy eget, consectetuer id, vulputate a, magna. Donec vehicula augue eu neque. Pellentesque habitant morbi tristique senectus et netus et malesuada fames ac turpis egestas. Mauris ut leo. Cras viverra metus rhoncus sem. Nulla et lectus vestibulum urna fringilla ultrices. Phasellus eu tellus sit amet tortor gravida placerat. Integer sapien est, iaculis in, pretium quis, viverra ac, nunc. Praesent eget sem vel leo ultrices bibendum. Aenean faucibus. Morbi dolor nulla, malesuada eu, pulvinar at, mollis ac, nulla. Curabitur auctor semper nulla. Donec varius orci eget risus. Duis nibh mi, congue eu, accumsan eleifend, sagittis quis, diam. Duis eget orci sit amet orci dignissim rutrum.

Nam dui ligula, fringilla a, euismod sodales, sollicitudin vel, wisi. Morbi auctor lorem non justo. Nam lacus libero, pretium at, lobortis vitae, ultricies et, tellus. Donec aliquet, tortor sed accumsan bibendum, erat ligula aliquet magna, vitae ornare odio metus a mi. Morbi ac orci et nisl hendrerit mollis. Suspendisse ut massa. Cras nec ante. Pellentesque a nulla. Cum sociis natoque penatibus et magnis dis parturient montes, nascetur ridiculus mus. Aliquam tincidunt urna. Nulla ullamcorper vestibulum turpis. Pellentesque cursus luctus mauris.

Contents

| | |
|--|------------|
| Acknowledgements | i |
| Abstract (English/Français/Deutsch) | iii |
| 1 Introduction | 1 |
| 1.1 Outline and Contribution | 1 |
| 1.2 Publications | 1 |
| 2 Safely learning with kernels | 3 |
| 2.1 The problem of learning | 3 |
| 2.2 The uncertainty quantification problem | 7 |
| 2.3 A sub-optimal closed-form solution | 12 |
| 3 Experimenting with Gaussian processes | 15 |
| 3.1 The control problem | 15 |
| 3.2 The building and its HVAC system | 15 |
| 3.3 The proposed solution | 16 |
| 3.4 Experimental results | 19 |
| 4 Learning MPC controllers with pQP neural networks | 23 |
| 4.1 pQP neural networks | 23 |
| 4.2 Learning linear MPC controllers with pQP neural networks | 23 |
| 4.2.1 The proposed architecture | 24 |
| 4.2.2 Properties of the approximator | 25 |
| 4.3 Simulation results | 27 |
| 4.4 Experimental results | 28 |
| 4.5 Learning a faithful still simpler representation of the controller . . | 31 |
| 4.5.1 The general architecture | 32 |
| A Elements of analysis and algebra | 35 |
| B Properties of kernels | 39 |

Contents

Bibliography **41**

Curriculum Vitae **43**

1 Introduction

A non-numbered chapter...

1.1 Outline and Contribution

1.2 Publications

The subsequent chapters of this dissertation were based on the following publications:

- E. T. Maddalena, Y. Lian, and C. N. Jones. "Data-driven methods for building control—A review and promising future directions." *Control Engineering Practice* 95 (2020): 104211.
- E.T. Maddalena, P. Scharnhorst, and C. N. Jones. "Deterministic error bounds for kernel-based learning techniques under bounded noise." *Automatica* 134 (2021): 109896.
- P. Scharnhorst, E.T. Maddalena, Y. Jiang, and C. N. Jones. "Robust Uncertainty Bounds in Reproducing Kernel Hilbert Spaces: A Convex Optimization Approach." arXiv.
- E. T. Maddalena, P. Scharnhorst, Y. Jiang, and C. N. Jones. "KPC: Learning-based model predictive control with deterministic guarantees." *Learning for Dynamics and Control*. PMLR, 2021.
- E. T. Maddalena, S. A. Müller, R. M. dos Santos, C. Salzmann, C. N. Jones. "Experimental Data-Driven Model Predictive Control of a Hospital HVAC System During Regular Use." *Energy and Buildings*: 112316 (2022).

Introduction

Works developed during the course of this PhD that are related to the thesis, but not discussed herein include:

- E. T. Maddalena, M. W. F. Specq, V. L. Wisniewski, and C. N. Jones. "Embedded PWM predictive control of DC-DC power converters via piecewise-affine neural networks." *IEEE Open Journal of the Industrial Electronics Society* (2021): 199-206.
- E.T. Maddalena, and C. N. Jones. "NSM converges to a k-NN regressor under loose Lipschitz estimates." *IEEE Control Systems Letters* 134 (2020): 880-885.
- E. T. Maddalena, C. G. S. Moraes, G. Waltrich, and C. N. Jones. "A neural network architecture to learn explicit MPC controllers from data." *IFAC-PapersOnLine* (2020): 11362-11367.
- A. Chakrabarty, E. T. Maddalena, H. Qiao, and C. Laughman. "Scalable Bayesian optimization for model calibration: Case study on coupled building and HVAC dynamics." *Energy and Buildings* 253, 111460
- E. T. Maddalena, and C. N. Jones. "Learning non-parametric models with guarantees: A smooth Lipschitz regression approach." *IFAC-PapersOnLine* (2020): 965-970.
- U. Rosolia, Y. Lian, E. T. Maddalena, G. Ferrari-Trecate, and C. N. Jones "On the Optimality and Convergence Properties of the Iterative Learning Model Predictive Controller." *IEEE Transactions on Automatic Control*.
- L. di Natale, Y. Lian, E. T. Maddalena, J. Shi, and C. N. Jones "Lessons Learned from Data-Driven Building Control Experiments: Contrasting Gaussian Process-based MPC, Bilevel DeePC, and Deep Reinforcement Learning." *arXiv*.

2 Safely learning with kernels

In this chapter, we will introduce the problem of learning from data and elucidate what approach will be taken to tackle it. Next, novel uncertainty quantification results will be presented concerning the point-evaluations of an unknown ground-truth. Finally, some examples are given to illustrate the general use of the theory.

2.1 The problem of learning

At its core, learning refers to the process of *gathering information* and using it to *improve one's knowledge* about the subject or phenomenon under study. The standing assumption here is then clearly that a link is in place, tying information and phenomenon together, even if such link is partially corrupted.

Information comes in many science fields in the form of data, samples, sometimes referred to as examples. In modern machine learning, people study a number of rather abstract subjects ranging from the traits that distinguish images of muffins and chihuahuas, to the link between passengers' features and their survival likelihood in case of a ship sinking event. The mathematical formalism often used to study the link between examples and these phenomena is statistics. This choice is convenient because it can describe the possible non-determinism of outcomes through the concepts of distributions and samples; and because it provides us with plenty of tools to carry out learning, i.e., improve our knowledge about the phenomenon through the samples at hand. In this chapter, we will however adopt a different standpoint to study and tackle the problem of learning, which is, as we will later argue, more aligned with the ways control engineers are taught to see physical systems. This standpoint is the one offered by approximation theory.

Statistical learning and approximation theory are not in opposition. Indeed, we can

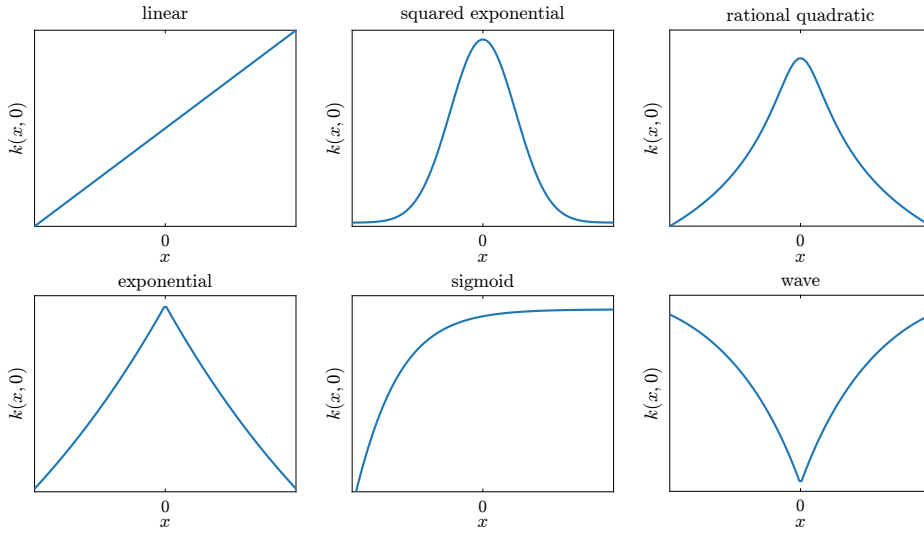


Figure 2.1: Examples of positive-definite kernels.

define the function of interest as the conditional Temlyakov (2008), perhaps talk about Belkin's work linking the two and advocating for using the approximation lenses.

Definition 1. (Kernel) Given an arbitrary non-empty set \mathcal{X} , a kernel k is any symmetric function of the form

$$k : \mathcal{X} \times \mathcal{X} \rightarrow \mathbb{R} \quad (2.1)$$

Definition 2. (Kernel matrix) Let $X = \{x_1, \dots, x_n\} \subset \mathcal{X}$ be a finite set of points. The $n \times n$ matrix K_{XX} with entries $[K_{XX}]_{ij} = k(x_i, x_j)$ is called the kernel matrix of k associated with X .

Definition 3. (Positive-definite kernel) A kernel function k is said to be positive-definite if for any finite subset of points $X \subset \mathcal{X}$, the kernel matrix satisfies $K_{XX} \succeq 0$. If, in particular, $K_{XX} > 0$, then the kernel is strictly positive-definite.

Aside from the last definition, we underline that there exist broader classes of kernel functions such as the *conditionally positive-definite* one (Schölkopf and Smola, 2002, §2.4)(Wendland, 2004, §8). In this chapter however, our attention will be focused on the positive-definite (PD) set, from which some examples are shown in Figure 2.1. A more complete list of PD kernels and their mathematical properties can be found in Appendix A.

Recall that our original goal was to learn functions $f : \mathcal{X} \rightarrow \mathbb{R}$. With a kernel at hand, one can define functions with the same domain and co-domain simply by

partially evaluating k , in other words, fixing one of its arguments: for some $z \in \mathcal{X}$, we can define $k(z, \cdot) : \mathcal{X} \rightarrow \mathbb{R}, x \mapsto k(z, x)$. Indeed, this was the approach taken to draw the plots in Figure 2.1. Approximating the unknown ground-truth with a single partially evaluated kernel however appears to be overly restrictive. The next logical step is to consider a larger hypothesis space where our approximation is given by a linear combination of such kernel functions. It turns out that every PD kernel already has a similar space associated with it, which is complete and endowed with enough structure to allow us to develop our uncertainty quantification theory. The following concepts are presented next to set up the stage for defining this special hypothesis space, the *reproducing kernel Hilbert space*.

Talk about feature maps, liftings and their importance.

Proposition 1. (PD kernels have feature maps) Let $k : \mathcal{X} \times \mathcal{X} \rightarrow \mathbb{R}$ be a positive-definite kernel. Then there exists a Hilbert space \mathbb{H} endowed with an inner product $\langle \cdot, \cdot \rangle_{\mathbb{H}}$ and a mapping $\Phi : \mathcal{X} \rightarrow \mathbb{H}$ such that

$$k(x, x') = \langle \Phi(x), \Phi(x') \rangle_{\mathbb{H}} \quad (2.2)$$

holds for any $x, x' \in \mathcal{X}$.

Proof: (Steinwart and Christmann, 2008, Theorem 4.16), modulo the nomenclature difference. \square

The mappings Φ above as well as the \mathbb{H} spaces are in general not unique (Steinwart and Christmann, 2008, §4), but there is one such space that enjoys an extra property that rules out some unexpected behavior from its members. This concept is introduced next.

Definition 4. (Reproducing kernel Hilbert space) Let $\mathcal{X} \neq \emptyset$ and $\mathbb{R}^{\mathcal{X}}$ the set of functions mapping \mathcal{X} to \mathbb{R} . The subset $\mathcal{H} \subset \mathbb{R}^{\mathcal{X}}$ is called a reproducing kernel Hilbert space (RKHS) if it is a Hilbert space and if $\forall x \in \mathcal{X}$ the evaluation functionals

$$L_x : \mathcal{H} \rightarrow \mathbb{R}, L_x(f) \mapsto f(x), \forall f \in \mathcal{H} \quad (2.3)$$

are bounded.

In order to see how useful such a property is, consider a sequence $\{f_n\}_{n=1}^{\infty}$ within a certain Hilbert function space $\mathbb{H} \subset \mathbb{R}^{\mathcal{X}}$. Intuitively, one would expect that if $f_n \rightarrow f^*$ in \mathbb{H} , then the values $f_n(x)$ attained by the sequence would converge to the values $f^*(x)$. Yet, this is not always the case (see Example 1 in Appendix A). If, on the other hand, the evaluation functionals are bounded as in Definition 4, then the connection between convergence in the function space and the pointwise

convergence of functions is guaranteed. Indeed, if $\{f_n\}_{n=1}^{\infty}$ and f^* are members of an RKHS \mathcal{H} , then $|f_n(x) - f^*(x)| = |L_x(f_n) - L_x(f^*)| \leq \|L_x\| \|f_n - f^*\|_{\mathcal{H}}$. $\|L_x\|$ is the operator norm of L_x , which is guaranteed by Definition 4 to be a finite number, and $\|f_n - f^*\|_{\mathcal{H}} \rightarrow 0$. Therefore, function convergence in an RKHS implies pointwise convergence, matching our intuition.

Proposition 2. (Every RKHS has a unique PD reproducing kernel) Let $\mathcal{H} \subset \mathbb{R}^{\mathcal{X}}$ be an RKHS. Then, the map $k : \mathcal{X} \times \mathcal{X} \rightarrow \mathbb{R}$, $k(x, x') := \langle L_x, L_{x'} \rangle_{\mathcal{H}}$ is a positive-definite kernel. Furthermore, k is the unique map to satisfy the reproducing property, i.e., for any $x \in \mathcal{X}$, $k(x, \cdot) \in \mathcal{H}$ and

$$\langle f, k(x, \cdot) \rangle_{\mathcal{H}} = L_x(f) = f(x), \quad \forall f \in \mathcal{H} \quad (2.4)$$

Proof: (Berlinet and Thomas-Agnan, 2011, Lemma 2) along with (Steinwart and Christmann, 2008, Theorem 4.20). \square

Proposition 3. (Every PD kernel has a unique RKHS) Let $k : \mathcal{X} \times \mathcal{X} \rightarrow \mathbb{R}$ be a PD kernel. If k is the reproducing kernel of an RKHS \mathcal{H}_A and of another RKHS \mathcal{H}_B , then $\mathcal{H}_A = \mathcal{H}_B$.

Proof: (Steinwart and Christmann, 2008, Theorem 4.21). \square

Despite being part of their name, it is not clear from the definition above what the relationship between RKHSs and kernels is. To shed light on the matter, it helps to explicitly construct \mathcal{H} starting from a given k . Consider the so-called *pre-Hilbert space*

$$\mathcal{H}_0 := \text{span} \{k(x, \cdot) \mid x \in \mathcal{X}\} \quad (2.5)$$

$$= \left\{ \sum_{i=1}^n c_i k(x_i, \cdot) \mid n \in \mathbb{N}, c_i \in \mathbb{R}, x_i \in \mathcal{X} \right\} \quad (2.6)$$

equipped with the real-valued map $\langle f, g \rangle_{\mathcal{H}_0} := \sum_{i=1}^n \sum_{j=1}^m a_i b_j k(x_i, x_j)$, which can be shown to be a valid inner-product, for members $f, g \in \mathcal{H}_0$, $f = \sum_{i=1}^n a_i k(x_i, \cdot)$, $g = \sum_{j=1}^m b_j k(x_j, \cdot)$. This family \mathcal{H}_0 of functions is however not guaranteed to be complete, i.e., sequences $\{f_i\}_{i \in \mathbb{N}}$ of members might converge to functions outside \mathcal{H}_0 . To transform it into a proper Hilbert space, one closes the space

$$\mathcal{H} := \text{clos } \mathcal{H}_0 \quad (2.7)$$

thus encompassing all limit points¹. Finally, the function space \mathcal{H} defined in (2.7)

¹Closing \mathcal{H}_0 requires defining an inner-product on the superset \mathcal{H} that is consistent with the

2.2 The uncertainty quantification problem

can then be shown to be a valid RKHS² according to Definition 4, in fact, the only RKHS associated with k . We therefore understand that the members of \mathcal{H} are weighted sums of partially evaluated kernels as per (2.6) along with their limit points.

Definition 5. (Universal kernel) Let k be a continuous PD kernel and the set \mathcal{X} be a compact metric space. Then k is called universal if its RKHS $\mathcal{H} \subset \mathbb{R}^{\mathcal{X}}$ is dense in the space of real-valued continuous functions $C(\mathcal{X}) \subset \mathbb{R}^{\mathcal{X}}$ with respect to the maximum norm $\|\cdot\|_{\infty}$.

From the above definition it follows that for any tolerable error $\epsilon > 0$, there exists an f in the RKHS of a universal kernel such that the discrepancy bounded $\|f(x) - g(x)\|_{\infty} \leq \epsilon$. Other model classes in machine learning are also known to be universal as defined above such as certain architectures of deep neural networks (Kidger and Lyons, 2020). All in all, the universality property is an indication of how rich a hypothesis space is, thus reassuring the user that little bias error will be introduced by his model class choice.

Proposition 4. Let \mathcal{X} be a compact subset of \mathbb{R}^n . The following are universal kernels

$$k(x, x') := \exp(\langle x, x' \rangle) \quad (2.8)$$

$$k(x, x') := \exp\left(-\frac{\|x - x'\|_2^2}{2\gamma^2}\right) \quad (2.9)$$

where $\gamma > 0$ and $\langle \cdot, \cdot \rangle$ is the usual inner-product on \mathbb{R}^n .

Proof: (Steinwart and Christmann, 2008, Corollary 4.58). \square

Discuss Steinwart et al. (2006) and also Steinwart (2020) when talking about the expressiveness of H. Universal kernels Micchelli et al. (2006)

2.2 The uncertainty quantification problem

Herein we consider a positive-definite kernel $k : \mathcal{X} \times \Omega \rightarrow \mathbb{R}$ along with its corresponding RKHS $\mathcal{H} \subset \mathbb{R}^{\Omega}$. Our input space is taken to be a compact subset of the Euclidean space $\Omega \subset \mathbb{R}^n$.

one present in the subset \mathcal{H}_0 . Also, the closure of a set is always closed, which guarantees that sequences within \mathcal{H} cannot converge to functions outside of it.

²For a proof of this statement, the reader is referred to (Berlinet and Thomas-Agnan, 2011, §3), or to (Sejdinovic and Gretton, 2012, §4) for a more step-by-step pedagogical exposition.

Assumption 1. The kernel function k is strictly positive-definite and its RKHS \mathcal{H} contains the ground-truth f^* .

Assumption 2. An estimate $\Gamma \geq \|f^*\|_{\mathcal{H}}$ for the ground-truth norm is known.

A dataset $\{(x_i, y_i)\}_{i=1}^d$ is given to us, being composed of inputs $x_i \in \Omega$ and outputs $y_i \in \mathbb{R}^{n_i}$, $y_i = [y_{i,1} \dots y_{i,n_i}]^\top$ that contain n_i scalar samples collected at the same input location x_i . The dataset carries information about an underlying ground-truth map $f^* \in \mathcal{H}$ according to

$$y_{i,j} = f^*(x_i) + \delta_{i,j} \quad (2.10)$$

where $\delta_{i,j}$ represents an additive measurement noise that is assumed to be uniformly bounded **as stated next**.

Assumption 3. The magnitude of each noise realization $\delta_{i,j}$ is bounded by a known scalar quantity $\bar{\delta}$, i.e. $|\delta_{i,j}| \leq \bar{\delta}, \forall i, j$.

To upper bound the ground-truth values, we consider the following infinite-dimensional variational problem $\mathbb{P}0$, with the query point $x \in \Omega$ as a parameter

$$\boxed{F(x) = \sup_{f \in \mathcal{H}} \{f(x) : \|f\|_{\mathcal{H}} \leq \Gamma, \|fx - y\|_{\infty} \leq \bar{\delta}\}} \quad (2.11)$$

where $fx := \Lambda [f(x_1) \dots f(x_d)]^\top$ is the vector of evaluations at the input locations, which are repeated whenever multiple outputs are available at a given input. This is accomplished through Λ as defined in Appendix ???. We highlight that the supremum is guaranteed to exist thanks to (??). Given a query location x , $\mathbb{P}0$ yields the tightest upper bound for $f(x)$ over all members $f \in \mathcal{H}$ of our hypothesis space that are consistent with our dataset, as well as our knowledge on the ground-truth complexity $\|f\|_{\mathcal{H}} \leq \Gamma$. Note how linking the function evaluations fx and the outputs y plays a role analogous to conditioning stochastic processes on past observations in statistical frameworks.

Consider now the convex parametric quadratically-constrained linear program $\mathbb{P}1$

$$\boxed{C(x) = \max_{c \in \mathbb{R}^d, c_x \in \mathbb{R}} c_x} \quad (2.12)$$

$$\text{subj. to } \begin{bmatrix} c \\ c_x \end{bmatrix}^\top \begin{bmatrix} K_{XX} & K_{Xx} \\ K_{xX} & k(x, x) \end{bmatrix}^{-1} \begin{bmatrix} c \\ c_x \end{bmatrix} \leq \Gamma^2 \quad (2.13)$$

$$\|\Lambda c - y\|_{\infty} \leq \bar{\delta} \quad (2.14)$$

2.2 The uncertainty quantification problem

for any $x \in \Omega \setminus \{X\}$, and extend its value function to points $x = x_i \in X$ with the solution of $\mathbb{P}1' : C(x) = \max_{c \in \mathbb{R}^d} \{c_i \mid c^\top K_{XX}^{-1} c \leq \Gamma^2, \| \Lambda c - y \|_\infty \leq \bar{\delta}\}$. This can be thought of as finding a map that interpolates the points $\{(x_i, c_i)\}_{i=1}^d$ and maximizes its value c_x at the input location x . The two cases $\mathbb{P}1$ and $\mathbb{P}1'$ are distinguished due to the matrix in (2.13) becoming singular for any $x \in X$, and since it allows for one decision variable to be eliminated. Finally, the connection between (2.11) and (??) is stated next.

Theorem 1. (Finite-dimensional equivalence): The objective in $\mathbb{P}0$ attains its supremum in \mathcal{H} and $F(x) = C(x)$ for any $x \in \Omega$.

Proof: Let $\mathbb{X} := X \cup \{x\}$ and define the finite-dimensional subspace $\mathcal{H}^\parallel = \{f \in \mathcal{H} : f \in \text{span}(k(x_i, \cdot), x_i \in \mathbb{X})\}$. Furthermore, let $\mathcal{H}^\perp = \{g \in \mathcal{H} : \langle g, f^\parallel \rangle_{\mathcal{H}} = 0, \forall f^\parallel \in \mathcal{H}^\parallel\}$ be the orthogonal complement of \mathcal{H}^\parallel . Then, we have $\mathcal{H} = \mathcal{H}^\parallel \oplus \mathcal{H}^\perp$ and for all $f \in \mathcal{H}$, $\exists f^\parallel \in \mathcal{H}^\parallel, f^\perp \in \mathcal{H}^\perp : f = f^\parallel + f^\perp$. By employing the latter decomposition and using the reproducing property, we can reformulate $\mathbb{P}0$ in terms of \mathcal{H}^\parallel and \mathcal{H}^\perp as

$$\sup_{\substack{f^\parallel \in \mathcal{H}^\parallel \\ f^\perp \in \mathcal{H}^\perp}} \left\{ \langle f^\parallel + f^\perp, k(x, \cdot) \rangle_{\mathcal{H}} : \|f^\parallel + f^\perp\|_{\mathcal{H}}^2 \leq \Gamma^2, \|(f^\parallel + f^\perp)_X - y\|_\infty \leq \bar{\delta} \right\} \quad (2.15)$$

$$\stackrel{(i)}{=} \sup_{\substack{f^\parallel \in \mathcal{H}^\parallel \\ f^\perp \in \mathcal{H}^\perp}} \left\{ f^\parallel(x) : \|f^\parallel\|_{\mathcal{H}}^2 + \|f^\perp\|_{\mathcal{H}}^2 \leq \Gamma^2, \|f_X^\parallel - y\|_\infty \leq \bar{\delta} \right\} \quad (2.16)$$

$$\stackrel{(ii)}{=} \sup_{f^\parallel \in \mathcal{H}^\parallel} \left\{ f^\parallel(x) : \|f^\parallel\|_{\mathcal{H}}^2 \leq \Gamma^2, \|f_X^\parallel - y\|_\infty \leq \bar{\delta} \right\} \quad (2.17)$$

In (i), the f^\perp component vanished from the cost and from the last constraint due to orthogonality w.r.t. $k(x_i, \cdot) \in \mathcal{H}^\parallel$ for any $x_i \in \mathbb{X}$; moreover, the Pythagorean relation $\|f\|_{\mathcal{H}}^2 = \|f^\parallel\|_{\mathcal{H}}^2 + \|f^\perp\|_{\mathcal{H}}^2$ was also used. To arrive at the second equality (ii), one only has to note that the objective is insensitive to f^\perp and that any $f^\perp \neq 0_{\mathcal{H}}$ would tighten the first constraint.

The attainment of the supremum is addressed next. Consider (2.17) and denote the members of \mathcal{H}^\parallel simply as f . $\|f\|_{\mathcal{H}}^2 \leq \Gamma^2$ is a closed and bounded constraint as it is the sublevel set of a norm. We transform $\|f_X - y\|_\infty \leq \bar{\delta}$ into $|f(x_i) - y_{i,j}| \leq \bar{\delta}$, $i = 1, \dots, d$, $j = 1, \dots, n_i$. Sets of the form $\{a \in \mathbb{R} : |a| \leq b\}$ are clearly closed in \mathbb{R} , hence $\{f(x_i) \in \mathbb{R} : |f(x_i) - y_{i,j}| \leq \bar{\delta}, \forall i, j\}$ is also closed. For any x_i , the evaluation functional $L_{x_i}(f) = f(x_i)$ is a linear operator and thus pre-images of closed sets are also closed. Consequently, $\{f \in \mathcal{H}^\parallel : |f(x_i) - y_{i,j}| \leq \bar{\delta}, \forall i, j\}$ is closed in \mathcal{H}^\parallel . The intersection of a finite number of closed sets is necessarily

closed, thus all constraint present in (2.17) define a closed feasible set. Since \mathcal{H}^\parallel is finite-dimensional, any closed and bounded subset of it is compact (Heine–Borel); therefore, the continuous objective $L_x(f) = f(x)$ in (2.17) attains a maximum by the Weierstrass extreme value theorem.

Finally, we establish the connection between P0 and P1. From the above arguments, an optimizer for P0 must lie in \mathcal{H}^\parallel . The members $f \in \mathcal{H}^\parallel$ have the form $f(z) = \alpha^\top K_{\mathbb{X}z}$, being defined by the α weights. Due to the positive-definiteness of K , there exists a bijective map between outputs at the \mathbb{X} locations $f_{\mathbb{X}} = [f(x_1) \dots f(x_d) f(x)]^\top$ and the weights α , namely $\alpha = K_{\mathbb{X}\mathbb{X}}^{-1} f_{\mathbb{X}}$. $K_{\mathbb{X}\mathbb{X}}$ denotes the kernel matrix associated with the set $\mathbb{X} = X \cup \{x\}$. Consequently, optimizing over $f \in \mathcal{H}^\parallel$ is equivalent to optimizing over $[f(x_1) \dots f(x_d) f(x)]^\top =: [c^\top c_x]^\top$. The bounded norm condition can be recast as $\|f\|_{\mathcal{H}}^2 = \langle f, f \rangle_{\mathcal{H}} = \alpha^\top K_{\mathbb{X}\mathbb{X}} \alpha = [c^\top c_x] K_{\mathbb{X}\mathbb{X}}^{-1} [c^\top c_x]^\top$. The remaining constraint and the objective are straightforward. Noting that this reformulation is valid for any $x \in \Omega$ concludes the proof. \square

Given our knowledge on the noise influence $\bar{\delta}$, it is natural to ask what the limits of the uncertainty quantification technique considered herein are. For example, is the width of the envelope $C(x) - B(x)$ restricted to a certain minimum value that cannot be reduced even with the addition of new data? From (??), it is clear that at any input location $x_i \in X$, $C(x_i)$ and $B(x_i)$ cannot be more than $2\bar{\delta}$ apart. In addition to that, the presence of the complexity constraint (??) can bring the two values closer to each other. Depending on how restrictive this latter constraint is for a given x_i , the corresponding output y_i might lie outside the interval between $C(x_i)$ and $B(x_i)$. In this case, the resulting width is considerably reduced as illustrated in Figure 2.2 (left).

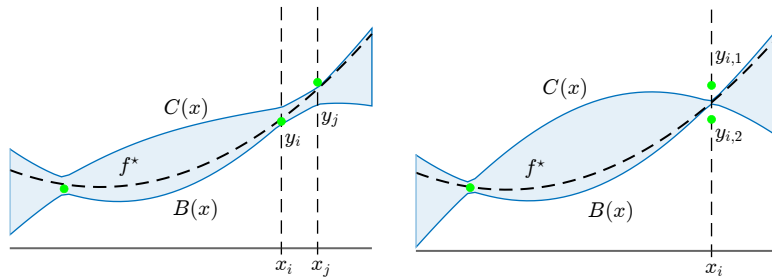


Figure 2.2: (Left) A sample lying outside of the uncertainty envelope, implying that the width is smaller than $\bar{\delta}$ at x_j . (Right) Redundant information is used to shrink the uncertainty envelope. In this scenario, we recover the ground-truth value at x_i as $C(x_i) = B(x_i) = f^*(x_i)$.

2.2 The uncertainty quantification problem

Proposition 5. (Width smaller than the noise bound): If $\exists y_i$ such that $y_{i,j} > C(x_i)$ or $y_{i,j} < B(x_i)$ for some j , then $C(x_i) - B(x_i) \leq \bar{\delta}$.

Proof: Follows from $C(x_i) \geq B(x_i)$, $C(x_i) \leq y_{i,j} + \bar{\delta}$ and $B(x_i) \geq y_{i,j} - \bar{\delta}$ for any $i = 1, \dots, d$ and any $j = 1, \dots, n_i$. \square

Suppose now one has sampled (x_i, y_i) with $y_i = [y_{i,1} \ y_{i,2}]^\top$, $y_{i,1} = f^*(x_i) + \bar{\delta}$ and $y_{i,2} = f^*(x_i) - \bar{\delta}$. Then there is no uncertainty whatsoever about f^* at x_i since $f^*(x_i) = (y_{i,1} + y_{i,2})/2$ is the only possible value attainable by the ground-truth. This illustrates that the possibility of having multiple outputs at the same location allows for the uncertainty interval to shrink past the $\bar{\delta}$ width, and eventually even reduce to a singleton as shown in Figure 2.2 (right). Notwithstanding, the addition of a new datum to an existing dataset|be it in the form of a new output at an already sampled location or a completely new input-output pair|can only reduce the uncertainty.

Proposition 6. (Decreasing uncertainty): Let $C_1(x)$ denote the solution of $\mathbb{P}1$ with a dataset $D_1 = \{(x_i, y_i)\}_{i=1}^d$, and $C_2(x)$ the solution with $D_2 = D_1 \cup \{(x_{d+1}, y_{d+1})\}$. Then $C_2(x) \leq C_1(x)$ for any $x \in \Omega$.

Proof. Denote by $\mathbb{P}1_1$ the problem solved with D_1 and decision variables $[c \ c_x]$. Similarly, $\mathbb{P}1_2$ is associated with the dataset D_2 and the decision variables $[c \ c_x \ c_z]$, where c_z are due to the additional input in D_2 . Since D_2 contains all members of D_1 , the ∞ -norm constraint of $\mathbb{P}1_2$ can be recast as that of $\mathbb{P}1_1$ and an additional constraint for c_z and the new outputs. Let $\bar{X} := X \cup \{x\}$, $\bar{c} := [c^\top \ c_x]^\top$ and $z := x_{d+1}$ be shorthand variables to ease notation. The complexity constraint of $\mathbb{P}1_2$ is then

$$\begin{bmatrix} \bar{c} \\ c_z \end{bmatrix}^\top \begin{bmatrix} K_{\bar{X}\bar{X}} & K_{\bar{X}z} \\ K_{z\bar{X}} & k(z, z) \end{bmatrix}^{-1} \begin{bmatrix} \bar{c} \\ c_z \end{bmatrix} \leq \Gamma^2 \quad (2.18a)$$

$$\stackrel{(i)}{\Leftrightarrow} \bar{c}^\top K_{\bar{X}\bar{X}}^{-1} \bar{c} + P_{\bar{X}}^{-2}(z) \left\| \begin{bmatrix} K_{\bar{X}\bar{X}}^{-1} K_{\bar{X}z} \\ -1 \end{bmatrix} \begin{bmatrix} \bar{c} \\ c_z \end{bmatrix} \right\|_2^2 \leq \Gamma^2 \quad (2.18b)$$

$$\stackrel{(ii)}{\Leftrightarrow} \begin{bmatrix} c \\ c_x \end{bmatrix}^\top \begin{bmatrix} K_{XX} & K_{Xx} \\ K_{xX} & k(x, x) \end{bmatrix}^{-1} \begin{bmatrix} c \\ c_x \end{bmatrix} + P_{\bar{X}}^{-2}(z) (\bar{c}^\top K_{\bar{X}\bar{X}}^{-1} K_{\bar{X}z} - c_z)^2 \leq \Gamma^2 \quad (2.18c)$$

where the matrix identity found in Appendix ?? was used in (i) and $P_{\bar{X}}^2(z) = k(z, z) - K_{z\bar{X}} K_{\bar{X}\bar{X}}^{-1} K_{\bar{X}z}$. In (ii), the definitions of \bar{c} and \bar{X} were used. Thanks to $P_{\bar{X}}(z) \geq 0, \forall z$ and the quadratic term multiplying it, we conclude that for any choice of the decision variable c_z , (2.18c) is a tightened version of the complexity constraint of $\mathbb{P}1_1$, which is (??). As a result, the maximum of $\mathbb{P}1_2$ is lower or

equal than that of $P1_1$. □

Let us take a closer look at the tightened constraint (2.18c). The term $\bar{c}^\top K_{\bar{X}\bar{X}}^{-1} K_{\bar{X}z} =: s(z)$ represents an interpolating model passing through the output values \bar{c} , that is, c and c_x (see e.g. the discussion in Section 3.1 of [?](#)). If the difference $s(z) - c_z$ can be made small, then the tightening will also be reduced, whereas it will be significant if the difference is large. The result is of course dictated by the ∞ -norm constraint, since c_z cannot be more than $\bar{\delta}$ away from all the outputs y available at z . Therefore, a new datum will cause significant shrinkage of the envelope at a point $z \in \Omega$ when the new output causes $s(z) - c_z$ to be large, which intuitively can be seen as a measure of gained information through the new sample. Finally, this process is weighted by the inverse of the power function $P_{\bar{X}}^{-2}(z)$, which does not depend on any output, but only on the input locations. This indicates the advantage of evenly-spaced samples over random or bulked ones on the overall bound width. Example 1 in Section [??](#) confirms this intuition.

Remark 1. Recovering the ground-truth as shown in Figure 2.2 (right) requires the noise realizations to match $\bar{\delta}$ and $-\bar{\delta}$; it is thus necessary to have tight noise bounds for it to happen. On the other hand, Proposition 6 guarantees the decreasing uncertainty property regardless of how accurate $\bar{\delta}$ is. Although not explicitly stated, a completely analogous result holds for the lower part of the envelope $B(x)$.

2.3 A sub-optimal closed-form solution

The discussion in this subsection assumes that only one sample is present at each input location, i.e., $y_i = y_i$ for $i = 1, \dots, d$, so that $y = y$.

In order to alleviate the computational complexity of having to solve two optimization problems at each query point, closed-form expressions can be employed instead. These surrogates yield sub-optimal bounds around any pre-specified kernel model of the form $s(x) = \alpha^\top K_{Xx}$, for some $\alpha \in \mathbb{R}^d$.

Proposition 7. Let $s(x) = \alpha^\top K_{Xx}$, for a given $\alpha \in \mathbb{R}^d$. Then, for any $x \in \Omega$, the ground-truth is bounded by $s(x) - S(x) \leq f^*(x) \leq s(x) + S(x)$ with

$$S(x) = P_X(x) \sqrt{\Gamma^2 + \tilde{\Delta}} + \bar{\delta} \|K_{XX}^{-1} K_{Xx}\|_1 + |\tilde{s}(x) - s(x)| \quad (2.19)$$

where $\tilde{s}(x) = y^\top K_{XX}^{-1} K_{Xx}$, and the constant $\tilde{\Delta}$ is the minimum of the unconstrained convex problem $\min_{\nu \in \mathbb{R}^d} \left\{ \frac{1}{4} \nu^\top K_{XX} \nu + \nu^\top y + \bar{\delta} \|\nu\|_1 \right\}$.

Proof. See Appendix ??.

□

The map $\tilde{s}(x) = y^\top K_{XX}^{-1} K_{Xx}$ is an interpolant for the available outputs y . Note also that none of the terms in (2.19) depend on the model weights α with the exception of the last term $|\tilde{s}(x) - s(x)|$. Therefore, the width $S(x)$ will be minimized when $s(x) = \tilde{s}(x) \implies \alpha = y^\top K_{XX}^{-1}$. Since such a model would severely overfit, a balance between smoothing the data and not diverging too much from $\tilde{s}(x)$ has to be found. In our previous work ?, we have illustrated how kernel ridge regression and minimum norm models are good candidate techniques to accomplish this goal.

By reformulating the optimal bounds, we uncover their relation with the suboptimal estimates given in Proposition 7. First, consider P1 and optimize over the decision variable $\delta = c - y$ rather than over c . Next, apply a quadratic decomposition identical to the one used in (2.18) to the complexity constraint (??) and solve for c_x . After recalling that $\tilde{s}(x) = y^\top K_{XX}^{-1} K_{Xx}$ and $\|\tilde{s}\|_{\mathcal{H}}^2 = y^\top K_{XX}^{-1} y$, one obtains

$$c_x \leq P(x) \sqrt{\Gamma^2 - \|\tilde{s}\|_{\mathcal{H}}^2 - \delta^\top K_{XX}^{-1} \delta + 2y^\top K_{XX}^{-1} \delta} + \tilde{s}(x) + \delta^\top K_{XX}^{-1} K_{Xx} \quad (2.20)$$

Instead of maximizing c_x , the right-hand side of (2.20) can be directly considered as the objective function equivalently. As a result, we obtain

$$\max_{\|\delta\|_\infty \leq \bar{\delta}} \tilde{s}(x) + P(x) \sqrt{\Gamma^2 - \|\tilde{s}\|_{\mathcal{H}}^2 - \delta^\top K_{XX}^{-1} \delta - 2y^\top K_{XX}^{-1} \delta + \delta^\top K_{XX}^{-1} K_{Xx}}$$

Now, relax the problem by allowing δ to attain different values inside and outside the square-root

$$\begin{aligned} & \max_{\delta_1, \delta_2 \in \mathbb{R}^d} \tilde{s}(x) + P(x) \sqrt{\Gamma^2 - \|\tilde{s}\|_{\mathcal{H}}^2 - \delta_1^\top K_{XX}^{-1} \delta_1 + 2y^\top K_{XX}^{-1} \delta_1 + \delta_2^\top K_{XX}^{-1} K_{Xx}} \\ & \text{subj. to } \|\delta_1\|_\infty \leq \bar{\delta}, \|\delta_2\|_\infty \leq \bar{\delta} \end{aligned} \quad (2.21a)$$

Note that the objective is separable and that $\tilde{\Delta}$ is the dual solution of

$$\max_{\delta_1 \in \mathbb{R}^d} \left\{ -\delta_1^\top K_{XX}^{-1} \delta_1 + 2y^\top K_{XX}^{-1} \delta_1 - \|\tilde{s}\|_{\mathcal{H}}^2 \right\} \quad (2.22)$$

Also, $\max_{\delta_2 \in \mathbb{R}^d} \{\delta_2^\top K_{XX}^{-1} K_{Xx} : \|\delta_2\|_\infty \leq \bar{\delta}\} = \bar{\delta} \|K_{XX}^{-1} K_{Xx}\|_1$ since these norms are duals of each other. Remember that the objective (2.21a) is a conservative upper bound for $f^*(x)$, having $\tilde{s}(x)$ as the reference model. Given any smoother $s(x)$, the triangle inequality $|f(x) - s(x)| \leq |f(x) - \tilde{s}(x)| + |\tilde{s}(x) - s(x)|$ can be used to bound the distance between its predictions and the ground-truth values, arriving thus at the same expressions presented in Proposition 7.

From (2.20), the noise variable δ is seen to increase the maximum in two distinct ways: through the inner product $\delta^\top K_{XX}^{-1} K_{Xx}$, and via a norm augmentation corresponding to $\tilde{\Delta}$. One source of conservativeness in Proposition 7 is taking into account the worst-possible inner-product and norm increase jointly. Despite this fact, they yield competitive results for moderate noise-levels as shown numerically in Section ???. We moreover note that in the noise-free scenario, (2.20) and (2.21a) are the same, and Proposition 7 simplifies to the classical bounds in the interpolation case (see for instance ?).

Remark 2. The sub-optimal bounds presented in this subsection feature a nominal model at their center, which is desirable in many practical situations. In the optimal scenario, the minimum norm regressor $s^*(x) = \alpha^{*\top} K_{Xx}$, $\alpha^* = \arg \min_{\alpha \in \mathbb{R}^d} \{\alpha^\top K_{XX}\alpha : \|K_{XX}\alpha - y\|_\infty \leq \bar{\delta}\}$ can be used as a nominal model. This choice is guaranteed to lie completely within $C(x)$ and $B(x)$ although not necessarily in the middle|since the map s^* belongs to \mathcal{H} and is a feasible solution for P0.

3 Experimenting with Gaussian processes

In this chapter, we discuss the problem of learning and elucidate what viewpoint will be taken to tackle it. Next, novel results are presented concerning uncertainty estimation in a kernelized setting. Finally, some examples are given to illustrate the general use of the theory.

3.1 The control problem

3.2 The building and its HVAC system

The building considered in this study was a surgery center situated in the São Julião hospital complex, in the city of Campo Grande, MS, Brazil (Figure ??, left). The 51 rooms that compose it are in permanent use and, for information purposes, 528 surgical procedures were carried out in it during August 2021. We were concerned with three thermal zones in its ophthalmology section: two operating rooms (ORs) and one waiting room (WR), all located on the West end of the building (Figure ??, right). Whereas the former rooms are only connected to the waiting room, the latter has a door to the rest of the surgery center. Opaque glass bricks are present in the waiting room as can be seen in the picture, allowing some natural light to enter the space; the operating rooms on the other hand do not feature them, nor do they have any windows. All spaces have exterior walls, but the right-hand side operating room is significantly more affected by direct solar radiation due to the disposition of the nearby trees.

A forced-air HVAC plant is in place to provide the occupants with a suitable indoor climate in accordance with local regulations. A total of seven air-handling units (AHUs) collect outdoor air that is then treated and filtered before being pumped into the several indoor spaces. We had control only over three AHUs, one

for each aforementioned thermal zone. A central chiller connected to an external cooling tower provides chilled water to all AHUs, which in turn feature three-way valves to control the flow of water through their cooling coils. The AHU fans are operated always at constant speed, resulting in a constant volumetric flow through the air-ducts and into the zones. As per the regulations, no air recycling is possible and all return air is directly discharged into the atmosphere. As the temperature in Campo Grande is typically high, the HVAC system was conceived to only cool the space, not having the means to provide positive thermal energy (for more details, see Section ??).

Two distinct sensor networks were deployed to monitor the HVAC plant and the indoor spaces. Firstly, we will describe the one located in the AHU room. One local controller (LCO)—a National Instruments myRIO—was attached to each air-handling unit, reading all sensors used to monitor the AHUs: supply and return water temperature probes, a water flow meter, an anemometer, as well as an angular position sensor. The LCOs were moreover responsible for running low-level signal processing routines and implementing control actions, i.e., acting on the three-way valve servomotor to change the chilled water flow, hence influencing the supply air temperature. Photos of the AHU room are shown in Figure 3.2. Next, in order to measure the indoor temperatures in a flexible way, a wireless network of Z-wave sensors was set up in the operating rooms and waiting room. These were equipped with external temperature probes (Dallas DS18B20) to guarantee fast and precise readings, reporting their measurements periodically to a local computer (LC) that featured a Z-wave transceiver attached to it.

A 3 GHz, 16 GB RAM, core i7 machine was installed in the waiting room, acting as the main computer platform for the project, i.e., the LC. This computer and the AHU LCOs were all connected to a local area network to exchange information, which was done by using the UDP protocol at a rate of approximately 1 Hz. Lastly, a weather station was deployed on site to measure the outdoor temperature and the solar radiation acting on the building with high accuracy. All signals were sampled with a period of two mins and stored into a local time-series database, InfluxDB. A block-diagram of the complete system is depicted in Figure ??.

3.3 The proposed solution

Given the learned GP models μ_i , $i = 1, 2, 3$ described in (??), a given maximum temperature T_{\max} , and our reconstructed electrical power surface, we formulate the following optimization problem to control the valves θ_i while reducing the

3.3 The proposed solution



Figure 3.1: Photos of the AHU room depicting the air ducts (top), the supply and return water pipes (top and bottom), and the three-way valve servomotor (bottom).

chiller energy consumption E_t

$$\min \quad \sum_{t=0}^{N-1} (E_t + \rho \Delta_t) + \rho_N \Delta_N \quad (3.1a)$$

$$\text{s.t.} \quad T_{t+1} = \mu(T_t, \theta_t, T_{\text{sup}}, T_{\text{out}}) \quad (3.1b)$$

$$T_t + \beta \text{ var}^{1/2}(T_t, \theta_t, T_{\text{sup}}, T_{\text{out}}) \leq T_{\max} + \delta_t \quad (3.1c)$$

$$E_t = Q(T_{\text{out}}, \Theta_t) / \text{COP}(Q(T_{\text{out}}, \Theta_t)) \quad (3.1d)$$

$$\theta_{\min} \leq \theta_t \leq \theta_{\max} \quad (3.1e)$$

$$\delta_t \geq 0 \quad (3.1f)$$

where $\Theta_t = \sum_{i=1}^3 \theta_{i,t}$ is the sum of all valve positions. The variables δ_t in (3.1c) are positive slacks introduced to avoid infeasibility. If needed, these can relax the temperature constraint so that the solver can return a viable control plan. Of course, their use is heavily penalized in the objective, where $\Delta_t = \sum_{i=1}^3 \delta_{i,t}^2$ and ρ , ρ_N are large constants, which in our case were respectively set to 100 and 200. The temperature constraint (3.1c) also accounts for prediction uncertainty as it includes the standard deviation $\text{var}^{1/2}$. Its use confers on the formulation a risk-aware quality and robustifies the closed-loop operation. The degree of conservativeness

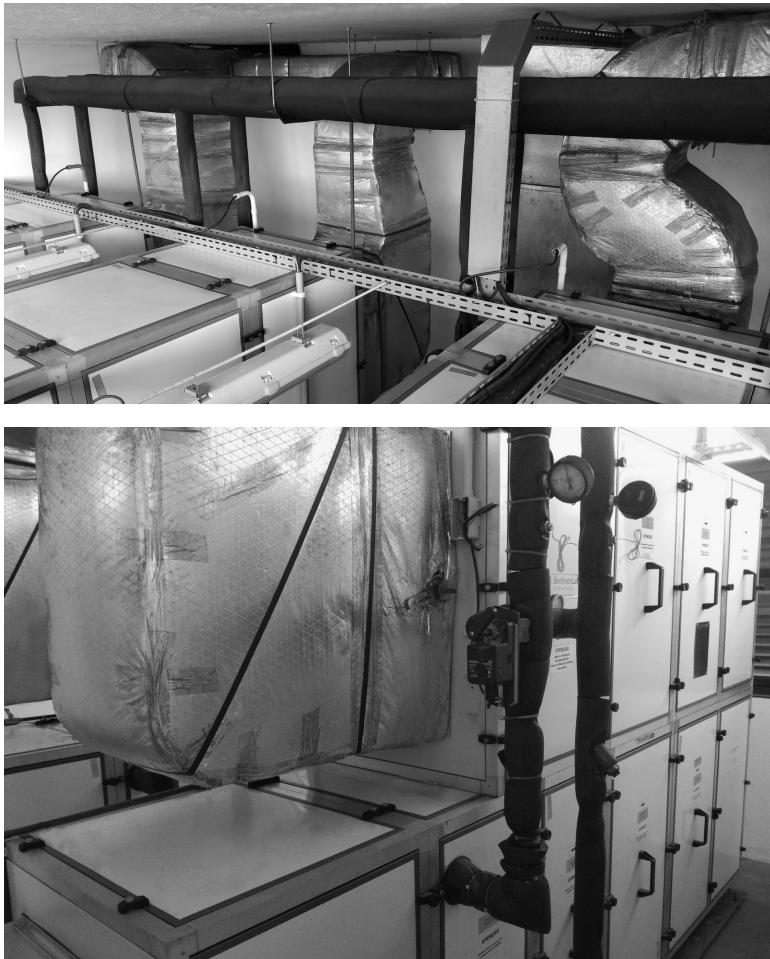


Figure 3.2: Photos of the AHU room depicting the air ducts (top), the supply and return water pipes (top and bottom), and the three-way valve servomotor (bottom).

is controlled by the constant β , chosen to be 2 as in Figure ???. The prediction horizon was set to $N = 12$ steps, which translates to 2 hours. As suggested by our notation, T_{out} and T_{sup} were kept constant throughout all prediction steps—but updated from one sampling period to the next. Finally, our maximum temperature value was $T_{\text{max}} = 21$ degrees Celsius.

The optimization problem (3.1) was written in **Python** with the aid of CasADi ?, an automatic-differentiation package that provides gradient information for numerical solvers—in our case, the interior-point method IPOPT. As is customary in predictive control, (3.1) was recursively solved on-line with the most recently available system information, with only the first optimal control action being transmitted to the valves. We underline that the main source of complexity in (3.1) is the presence of the constraints (3.1b) and (3.1c), which are highly non-

linear due the GP mean and variance. Since convexity is absent, multiple local optima might exist, a fact that was indeed verified in practice. By intelligently providing solvers with high-quality initial guesses, this problem can be mostly overcome. Our particular case study relied on initializing the numerical solver with control, temperature, slack and energy trajectories obtained with a virtual PI controller. The intuition was to allow the MPC loop to build on such an initial guess and further optimize operation. For a detailed study on solve times and how the number of GP data-points impacted them, see Appendix A.

3.4 Experimental results

The previously described Gaussian process-based MPC formulation was deployed on the local computer and used to operate the HVAC system during multiple days in the months of October and November 2021. We report in Figure 3.3 a four-day uninterrupted experiment carried out from November 10 to November 13 that is rather representative of the local internal and external conditions. The plots show the room temperatures and the “immediate” uncertainty associated with the GP predictions: $T_{\text{unc}} = \beta \text{var}^{1/2}$ as employed in the formulation (3.1c), and evaluated for the next time-step. Both outdoor signals, the temperature and the solar radiation, are also given. The reader is reminded that, although the latter contributes with additional heat gains, it is completely unknown to the controller as explained in Section ???. We highlight that the curves displayed in the figure were not filtered in any way; the sole manipulation performed with the data was the imputation of the missing temperature entries using linear interpolation. These points, however, accounted for only 43 out of the 1728 indoor temperature values gathered during the four-day experiment.

Consider first the day November 10 and note the relatively high internal room temperatures when the experiment started, which were the consequence of a harsh previous day. The MPC controller used some control authority to bring the temperatures below the 21-degree line and then partially closed the valves. After the morning shift started (7 am), even though θ_2 and θ_3 were fully open, T_2 and T_3 violated the constraints and were only brought below 21 degrees late that evening. High initial conditions along with a peak outdoor temperature of 35 degrees overloaded the cooling system, causing violations of the indoor temperature constraint in two rooms.

The two days that followed (November 12 and 13) were less warm and, as a result, the MPC controller successfully modulated the valves so as to guarantee constraint satisfaction. It is evident how θ_1 , θ_2 and θ_3 assume lower values when T_{out} is low,

Experimenting with Gaussian processes

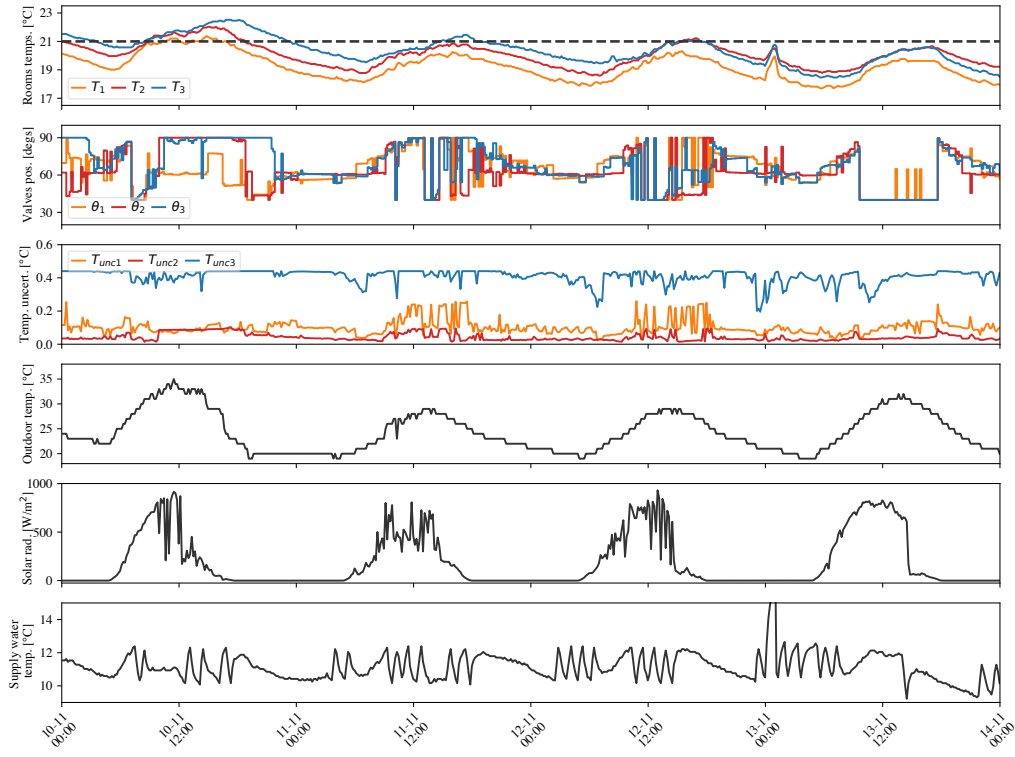


Figure 3.3: MPC experimental results over four days: indoor temperature, valve position and uncertainty estimate associated with each room (top three plots); outdoor temperature, solar radiation and AHUs supply water temperature (bottom three plots). The system was sampled and controlled with a periodicity of 10 minutes.

and tend to saturate at their maximum during working hours, which matches our intuition.

Lastly, we focus on the data from November 13, where one can readily see a sudden peak in the indoor temperatures, being also present in T_{sup} . This was caused by a momentary halt in the water pumps responsible for the chilled water circuit—an event that could be regarded as a fault from a control system perspective. During this period, as there was no water circulation through the AHU cooling coils, there was also no refrigeration and the indoor spaces received warm air since the fans were kept on. As soon as the pumps were again activated, the chiller immediately decreased the supply water temperature and the operation was normalized. During daytime, the indoor climate was kept within the desired limits despite the valves staying saturated at their low values, even at noon. The fact that almost no additional actuation was needed is due to that day being a Saturday, when no operations are scheduled and the three doors present in the environment are minimally opened and closed. This demonstrates how strong the

3.4 Experimental results

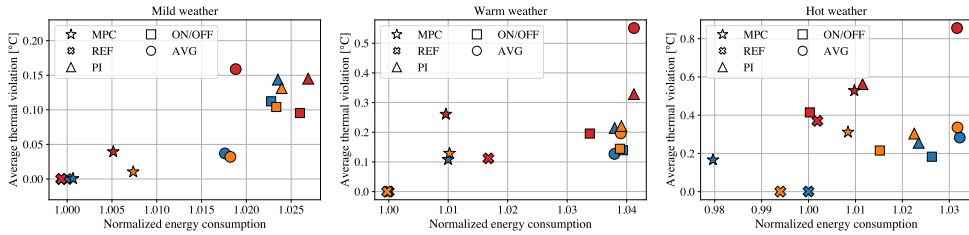


Figure 3.4: Simulation results of the normalized energy consumption and thermal performance (average temperature bound violation) of different control strategies. Three weather profiles were considered: mild, warm and hot. The indoor temperatures were initialized at different values according to the color scheme:...

internal heat gains and unmeasured disturbances normally are.

To assess the efficiency gains as well as the thermal performance of the deployed strategy, MPC was compared to alternative algorithms, all subject to exactly the same environmental conditions by means of simulations. We underline that this simulation model was calibrated on data that was *not* included in the GPs training set, thus putting to test the MPC prediction capabilities. The disturbance signals T_{out} , T_{sup} and R_{sol} from November 10 were employed, and the indoor temperatures of the three rooms were uniformly initialized at values ranging from 17 to 21 degrees Celsius. The outdoor temperature profile was processed to yield three different weather scenarios: hot weather, which was exactly the same T_{out} curve seen in Figure 3.3; warm weather, a -2°C shifted version of it, peaking at 33°C around noon; and mild weather, a -5°C shifted version of it, peaking at 30°C . Besides the MPC algorithm (3.1), the following were also tested:

- An MPC controller (herein referred to as REF) with perfect prediction capabilities, perfect disturbance information (T_{out} and T_{sup}) and a long prediction horizon of five hours.
- PI controllers featuring anti-windup schemes and feedforward components to enhance their performance.
- Rule-based ON/OFF controllers that set the valves respectively to θ_{\min} and θ_{\max} if the indoor temperatures were below or above the set-point.
- An average $(\theta_{\max} - \theta_{\min})/2$ controller (AVG) whose instantaneous values are selected by sampling the interval θ_{\min} to θ_{\max} using a uniform distribution.

In order to gauge the energy saving potential of the HVAC plant, we executed the REF strategy described above. This algorithm can reach significant efficiency

Experimenting with Gaussian processes

gains while guaranteeing thermal comfort since it exploits a perfect internal model as well as perfect forecasts of the outdoor and supply water temperatures.

The obtained normalized energy consumption results and average room thermal comfort violations are shown in Figure 3.4. Since the non-linear chiller curves described in Section ?? were employed to measure the energy consumption, the reader is reminded that there is a non-trivial relationship between the weather conditions and indoor temperatures, and the final consumed energy. This aspect is due to the nature of the chiller and not the use of any particular control technique. As a last note, one specific energy normalization factor was used for each weather scenario shown in Figure 3.4 to enhance clarity.

Glancing at the mild and warm weather plots, one notices how the REF and MPC data tended to be close together, and relatively far from the PI, ON/OFF and AVG clusters. Moreover, the REF and MPC points were also mostly to the left side and vertically below the other data given the same indoor temperature conditions—thus confirming their superior performance in terms of energy efficiency and indoor climate regulation. The ON/OFF and PI controllers yielded overall similar numerical results and, surprisingly, were outperformed by the AVG scheme under mild weather and starting indoor temperatures of 17°C and 19°C. AVG nevertheless performed poorly under warm weather and 21°C, and hot weather in general. All in all, the predictive control strategies MPC and REF yielded the best results in the mild and warm weather cases, whereas the separation among them and the other techniques became less evident under hot weather, indicating a less important advantage over classical control.

By analyzing the horizontal scales and contrasting REF to PI, ON/OFF and AVG, one concludes that this particular HVAC plant could have its efficiency boosted by approximately 2.5%, 4% and 5% respectively in the mild, warm and hot weather scenarios. Notice how, as opposed to studies such as ?, these numbers refer to the electrical energy associated with a chiller, and not to a cumulative thermal energy. Moreover, as the hospital was not subject to time-varying electricity prices, the contrast among control strategies was not as broad as for instance the one reported in ?. The proposed MPC strategy (3.1) attained results close to the aforementioned maximum percentages. Quantitatively, MPC lead to a maximum energy efficiency improvement of 2.29%, 3.13% and 4.76% respectively in mild, warm and hot weather, when compared to the PI and ON/OFF counterparts.

4 Learning MPC controllers with pQP neural networks

In this chapter, we ...

4.1 pQP neural networks

4.2 Learning linear MPC controllers with pQP neural networks

Consider the following standard MPC formulation for linear dynamical systems

$$\text{P1} : \min_{X,U} \quad \sum_{k=0}^{H-1} (x'_k Q x_k + u'_k R u_k) + x'_H P x_H \quad (4.1a)$$

$$\text{s.t.} \quad \forall k = 0, \dots, H-1 \quad (4.1b)$$

$$x_{k+1} = Ax_k + Bu_k \quad (4.1c)$$

$$x_k \in \mathbb{X} \quad (4.1d)$$

$$u_k \in \mathbb{U} \quad (4.1e)$$

$$x_H \in \mathbb{X}_H \quad (4.1f)$$

$$x_0 = x(0) \quad (4.1g)$$

where $X := \{x_1, \dots, x_H\}$, $U := \{u_0, \dots, u_{H-1}\}$, $Q \succeq 0$, $P \succeq 0$, $R \succ 0$, and the constraints are all described by affine equalities and inequalities. Denote by $\pi : \mathcal{X} \rightarrow \mathcal{U}$ the optimal solution of (4.18) in its parametric form with respect to the initial conditions $x(0)$, where $\mathcal{X} \subseteq \mathbb{R}^n$ is the feasible state space of P1 and $\mathcal{U} \subseteq \mathbb{R}^m$ is the control space. We assume a set of N samples can be acquired from

the original control law¹

$$D = \{\mathbf{x}_i, \mathbf{u}_i\}_{i=1}^N \quad (4.2a)$$

$$\mathbf{u}_i = \pi(\mathbf{x}_i), i = 1, \dots, N \quad (4.2b)$$

The process of acquiring the training dataset does not have to follow a particular distribution, nor do the samples have to be independent.

4.2.1 The proposed architecture

The key idea behind the proposed approximator is the use of a parametric quadratic program layer as part of the Neural Network, and optimizing over its parameters in order to fit the available dataset. This layer is implicitly described by the quadratic program

$$z^* = \arg \min_{z \geq 0} \|Lz + y_1(x)\|^2 + \epsilon \|z\|^2 \quad (4.3)$$

which is *always feasible* and *bounded from below*. The size of this mathematical program, i.e. the dimension of z , can be tuned to attain approximations with different complexity. Moreover, as notation suggests, the parameter y_1 depends on a previous affine layer that maps the system states into the z space, $y_1 := Fx + f$. Let $y_2 := z^*$, then another affine layer maps the optimal solution to the input space $y_3 := Gy_2 + g$, and a projection onto the feasible input set produces the final control action $\hat{u} := \text{Proj}_{\mathbb{U}}(y_2)$. This last step is necessary to guarantee feasibility of the control moves (see e.g. ??). An illustration of the proposed architecture is presented in Fig. ??, where the projection layer was particularized to a familiar element-wise saturation operation $\text{sat}(\cdot)$, valid for box input constraints.

Let the chosen number of decision variables in the pQP be $z \in \mathbb{R}^{n_z}$. We choose $L \in \mathbb{R}^{n_z \times n_z}$ to be square, and therefore $F \in \mathbb{R}^{n_z \times n}$, $f \in \mathbb{R}^{n_z}$. Moreover, $G \in \mathbb{R}^{m \times n_z}$ and $g \in \mathbb{R}^m$. If $n_z \geq n$, the first layer lifts the input data into a higher dimensional space before it is passed through the optimization layer. A last affine function then projects it onto the control space. These facts will be later employed to analyze the representative power of the network.

The parameters to be trained are therefore F , f , L , G and g . This process can be carried out via a stochastic gradient descent algorithm applied to an appropriate loss function. Differentiability of all layers is trivial with the exception of the pQP one (??). Regarding the latter, note that the objective in (4.3) can be rewritten

¹The dataset can also be directly obtained from the implicit controller; depending on the size of the problem at hand, computing the explicit solution might be intractable.

4.2 Learning linear MPC controllers with pQP neural networks

as

$$V(z) := z'(\epsilon I + L'L)z + (2L'y_1(x))'z + y_1(x)'y_1(x) \quad (4.4)$$

whose Lagrangian is simply

$$\mathcal{L}(z, \lambda) = V(z) - \lambda'z \quad (4.5)$$

The Karush-Kuhn-Tucker (KKT) conditions for primal and dual feasibility, complementary slackness, and stationarity then read

$$z^* \geq 0 \quad (4.6a)$$

$$\lambda^* \geq 0 \quad (4.6b)$$

$$\lambda_i^* z_i^* = 0, \forall i = 1, \dots, n_z \quad (4.6c)$$

$$2(\epsilon I + L'L)z^* + (2L'y_1(x)) - \lambda^* = 0 \quad (4.6d)$$

where λ_i and z_i denote the components of the Lagrange multipliers and decision variables vectors. The following proposition presents the differentiability properties of the pQP layer, and holds since (4.3) is a particular instance of the OptNet layer (?) with strictly convex objective function.

Proposition 8. Let $\theta := (L, y_1)$. The parametric solution $z^*(\theta)$ of (4.3) is subdifferentiable everywhere in its domain, i.e., $\partial z^*(\theta) \neq \{\}$, and $\partial z^*(\theta)$ has a unique element (the jacobian) everywhere but in a set of measure zero.

As shown in ?, the relevant gradients with respect to the parameters to be trained can be obtained from the KKT set of equations (4.6). Hence, backward passes are possible and backpropagation can be performed to optimize all of the NN parameters.

4.2.2 Properties of the approximator

The authors of ? showed that any continuous PWA function can be obtained as the solution of a particular parametric linear program (pLP) transformed by a linear map. Even though this view could be adopted herein, we instead prove a different result that is enough in the context of linear eMPC.

Theorem 2. (The proposed NN architecture can learn any linear quadratic MPC controller) Let $\hat{\pi} : \mathcal{X} \rightarrow \mathcal{U}$ be the map defined by the composition of all four layers, i.e., $\hat{\pi}(x) := y_4 \circ y_3 \circ y_2 \circ y_1(x)$. Set $\epsilon = 0$, then $\exists F, f, L, G$ and g with appropriate dimensions such that $\forall x \in \mathcal{X}$, $\hat{\pi}(x) = \pi(x)$.

Proof: Start by condensing the MPC problem P1, i.e., using the equality constraints

to eliminate all state decision variables except for the initial state $x(0)$. This leads to the following parametric problem

$$\mathbb{P}2 : \min_U U' \Lambda U + x(0)' \Gamma U \quad (4.7a)$$

$$\text{s.t. } \Phi U \leq \Omega x(0) + \omega \quad (4.7b)$$

The step by step procedure can be found in ?. We have that $\Lambda \succ 0$. Problems $\mathbb{P}2$ and $\mathbb{P}1$ are then equivalent in the sense that the solution U^* of $\mathbb{P}2$ and $\{X^*, U^*\}$ of $\mathbb{P}1$ share the same U^* component. Next, calculate the dual problem of $\mathbb{P}2$, which is

$$\mathbb{D}2 : \min_{\lambda \geq 0} \frac{1}{4} \left[\lambda' \Phi \Lambda^{-1} \Phi' \lambda + (4x(0)' \Omega' + 2x(0)' \Gamma \Lambda^{-1} \Phi' + 4\omega') \lambda + x(0)' \Gamma \Lambda^{-1} \Gamma' x(0) \right] \quad (4.8)$$

It is possible to recover the primal optimal solution U^* from the dual optimal solution λ^* through the stationarity optimality condition of $\mathbb{P}2$

$$U^* = -0.5 \Lambda^{-1} \Phi' \lambda^* - 0.5 \Lambda^{-1} \Gamma' x(0) \quad (4.9)$$

The above equation is learned by the second linear layer in Figure ???. Nevertheless, from (4.9) we see that it requires the value of $x(0)$, which is the NN input. It is shown next that with a pQP layer of appropriate size and parameters, it is possible not only to learn (4.8), but also let the value of $x(0)$ ‘pass through’ the NN and arrive to the second linear layer as needed to retrieve the primal optimal solution.

Let the auxiliary variable \tilde{L} and function $\tilde{y}_1(x) := \tilde{F}x + \tilde{f}$ be the solution to (compare (4.4) and (4.8))

$$\tilde{L}' \tilde{L} + \epsilon I = 0.25 \Phi \Lambda^{-1} \Phi' \quad (4.10a)$$

$$2\tilde{L}' \tilde{y}_1(x) = \Omega x(0) + 0.5 \Phi \Lambda^{-1} x(0) + \omega \quad (4.10b)$$

which leads to $\epsilon = 0$, $\tilde{L} = 0.5 (\Phi \tilde{\Lambda})'$, where $\tilde{\Lambda}$ is the unique square root of Λ^{-1} , guaranteed to exist as $\Lambda^{-1} \succ 0$. Then, $\tilde{y}_1(x) = (\Phi \tilde{\Lambda})^{-1} (\Omega x(0) + 0.5 \Phi \Lambda^{-1} x(0) + \omega) \implies \tilde{F} = (\Phi \tilde{\Lambda})^{-1} (\Omega + 0.5 \Phi \Lambda^{-1})$, $\tilde{f} = (\Phi \tilde{\Lambda})^{-1} \omega$.

Set the first layer weights to $F = [-I \ I \ \tilde{F}]'$ and $f = [\mathbf{0} \ \mathbf{0} \ \tilde{f}]'$ so that $y_1(x) = [-x; \ x; \ \tilde{F}x + \tilde{f}]$. Set the weights of the pQP layer (4.3) to $\epsilon = 0$ and $L = [I \ \mathbf{0} \ \mathbf{0}; \ \mathbf{0} \ I \ \mathbf{0}; \ \mathbf{0} \ \mathbf{0} \ \tilde{L}]$. If we partition the decision variable as $z = [\tilde{z} \ x^p \ x^n]'$, this results in

$$\min_{\tilde{z}, x^p, x^n \geq 0} \|x^p - x(0)\|^2 + \|x^n + x(0)\|^2 + \|\tilde{L}\tilde{z} + \tilde{y}_1(x)\|^2 \quad (4.11)$$

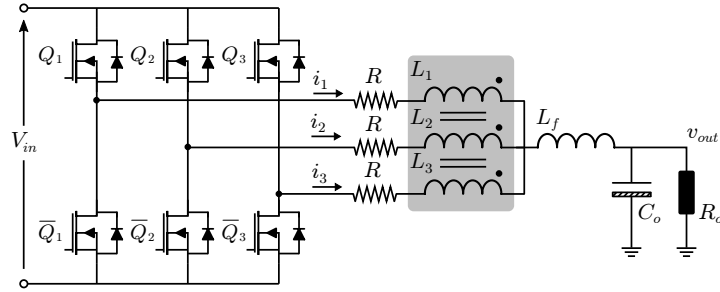


Figure 4.1: Photos of the AHU room depicting the air ducts (top), the supply and return water pipes (top and bottom), and the three-way valve servomotor (bottom).

which is a separable objective in \tilde{z} , \tilde{x}^p and \tilde{x}^n . Due to the choice of \tilde{L} and $\tilde{y}_1(x)$ in (4.10), the last term of the pQP matches the dual D2 with the exception of its constant term – not relevant for determining the optimal solution. Therefore, we have that \tilde{z}^* in (4.11) matches λ^* in D2. Regarding x^{p*} , the n optimizer components will satisfy $\forall i = 1, \dots, n$, $x_i^{p*} = x_i(0)$ if $x_i(0) \geq 0$, else $x_i^{p*} = 0$. Similarly, $x_i^{n*} = -x_i(0)$ if $x_i(0) \leq 0$, else $x_i^{n*} = 0$. Therefore, $x^{p*} - x^{n*} = x(0)$, and the output of the pQP layer (4.11) has the dual optimizer λ^* and the initial condition $x(0)$ encoded in it.

Next set the weights of the second linear layer y_3 to $G = [-0.5\Lambda^{-1}\Phi' \ -0.5\Lambda^{-1}\Gamma' \ 0.5\Lambda^{-1}\Gamma']$ and $g = \mathbf{0}$. Therefore, $y_3 = G[\tilde{z}^* \ x^{p*} \ x^{n*}]' = G[\lambda^* \ x^{p*} \ x^{n*}]' = U^*$, where equality (4.9) was used in the last step. Finally, note that the last layer $y_4 = \text{Proj}_{\mathbb{U}}(y_3)$ will simply evaluate to y_3 since y_3 is the optimal primal solution U^* , which satisfies the constraints (4.7b) and necessarily belongs to \mathbb{U} . The theorem then follows from the fact that $x(0)$ in the above calculations can be taken to be any point x in \mathcal{X} . \square

Exactly matching the original MPC controller would require L to have the same size of $\Phi\tilde{\Lambda}$ and $\epsilon = 0$ as shown. Nevertheless, we are interested precisely in reducing the complexity of the resulting controller through employing less parameters. In this process, choosing a regularizer $\epsilon > 0$ is beneficial since it ensures that the QP is bounded during the training phase for all possible parameters.

Comment: Stability certification

4.3 Simulation results

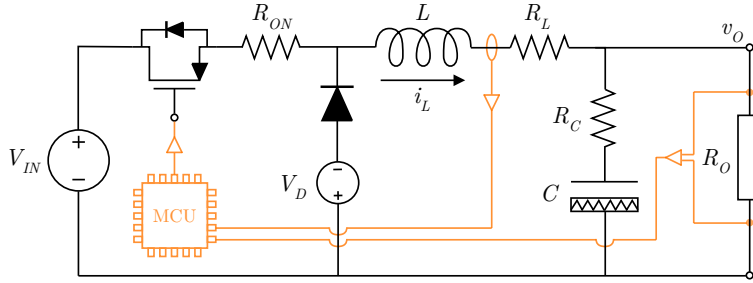


Figure 4.2: A circuit diagram of the buck converter including its parasitic resistances and the diode forward voltage drop. The feedback loop is closed by the MCU, which implements our proposed PWA-NN controller.

4.4 Experimental results

A schematic representation of the buck converter considered in this work is shown in Figure 4.2 and its parameters are found in Table ???. V_{IN} , V_D , L , and C refer respectively to the input voltage, the diode forward drop, the inductance and the capacitance; whereas R_{ON} , R_L , R_C and R_O refer to the switch on-resistance, the inductor parasitic resistance, the capacitor parasitic resistance, and the output load.

We choose as state variables the inductor current and the output voltage

$$x = \begin{bmatrix} x_1 \\ x_2 \end{bmatrix} = \begin{bmatrix} i_L \\ v_O \end{bmatrix} \quad (4.12)$$

The power switch is operated at a constant frequency f_{sw} and variable duty cycle, which is taken to be the control variable $u = \delta$. Following the classical time-averaging technique, Kirchhoff's circuit laws are used to derive differential equations for both when the switch is open, and when it is closed. The expressions can be found in Appendix ???. Averaging these equations with δ as a weight yields

Table 4.1: Parameters of the DC-DC converter

| V_{IN} | V_{OUT} | V_D | L | C | R_{ON} | R_L | R_C | R_O | f_{sw} |
|----------|-----------|-------|-------|------------|--------------|------------|----------------|--------------|----------|
| 15 V | 5 V | 0.1 V | 10 mH | 56 μ F | 5 m Ω | 2 Ω | 330 m Ω | 100 Ω | 20 kHz |

$$\dot{x}_1 = -\frac{R_L}{L}x_1 - \frac{1}{L}x_2 + \frac{V_{IN} + V_D}{L}u - \frac{R_{ON}}{L}x_1u - \frac{V_D}{L} \quad (4.13a)$$

$$\begin{aligned} \dot{x}_2 = & -\frac{R_C R_O R_L C + R_O L}{(R_C + R_O)LC}x_1 - \frac{R_C R_O C + L}{(R_C + R_O)LC}x_2 + \frac{R_C R_O (V_{IN} + V_D)}{(R_C + R_O)L}u \\ & - \frac{R_C R_O R_{ON}}{(R_C + R_O)L}x_1u - \frac{R_C R_O V_D}{(R_C + R_O)L} \end{aligned} \quad (4.13b)$$

The expressions above are not linear since the inductor current and the duty cycle multiply each other. As the goal is to design a linear MPC controller, linearization is needed. We first fix the output voltage to the desired value x_{2eq} and solve for the current and duty cycle steady-state values

$$x_{1eq} = \frac{x_{2eq}}{R_O} \quad (4.14)$$

$$u_{eq} = \frac{R_O V_D + (R_L + R_O)x_{2eq}}{R_O(V_{IN} + V_D) - R_{ON}x_{2eq}} \quad (4.15)$$

Finally, (4.13a) and (4.13b) are expanded around (x_{1eq}, u_{eq}) and the linear terms are kept, leading to the familiar state-space equations $\dot{x} = A_{ct}x + B_{ct}u$ where

$$A_{ct} = \begin{bmatrix} -\frac{R_L + R_{ON}u_{eq}}{L} & -\frac{1}{L} \\ -\frac{R_C R_O (R_L C - R_{ON}C u_{eq}) + R_O L}{(R_C + R_O)LC} & -\frac{R_C R_O C + L}{(R_C + R_O)LC} \end{bmatrix} \quad (4.16)$$

$$B_{ct} = \begin{bmatrix} \frac{V_{IN} + V_D - R_{ON}x_{1eq}}{L} \\ \frac{R_C R_O (V_{IN} + V_D - R_{ON}x_{1eq})}{(R_C + R_O)L} \end{bmatrix} \quad (4.17)$$

As a last step, a discrete-time model $x_{t+1} = Ax_t + Bu_t$ is obtained by integrating the continuous-time dynamics using the standard zero-order hold method. The chosen discretization frequency was $f_{\text{samp}} = 10 \text{ kHz}$, which is also the predictive controller frequency.

The goal is to attain a fast start-up response with as little overshoot as possible and regulate the output voltage v_O to $v_{eq} = 5 \text{ V}$. Furthermore, an inductor current constraint of 200 mA and voltage constraint of 7 V must be respected at all times. The prediction horizon has to be long enough to yield a large feasible set \mathcal{X} and we chose $N = 10$ steps. A standard quadratic objective was employed², penalizing the deviation of the states and control variable from the reference values

²In the MPC objective function, the squared weighted norms read as in $\|x_t - x_{\text{ref}}\|_Q^2 = (x_t - x_{\text{ref}})^\top Q (x_t - x_{\text{ref}})$.

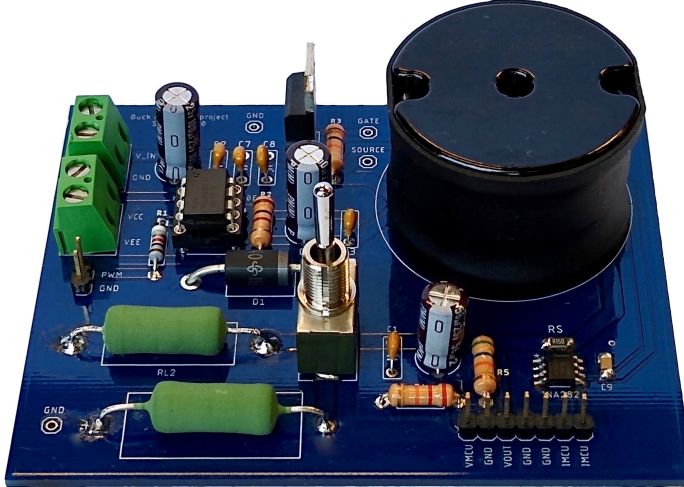


Figure 4.3: Photos of the AHU room depicting the air ducts (top), the supply and return water pipes (top and bottom), and the three-way valve servomotor (bottom).

$x_{\text{eq}} = \begin{bmatrix} 0.05 & 5 \end{bmatrix}^\top$, $u_{\text{eq}} = 0.3379$. The final optimal-control formulation was

$$\min_{X,U} \sum_{t=0}^{N-1} \left(\|x_t - x_{\text{eq}}\|_Q^2 + \|u_t - u_{\text{eq}}\|_R^2 \right) + \|x_N - x_{\text{eq}}\|_P^2 \quad (4.18a)$$

s.t. $\forall t = 0, \dots, N-1$

$$x_{t+1} = Ax_t + Bu_t \quad (4.18b)$$

$$\begin{bmatrix} i_L^{\min} \\ v_O^{\min} \end{bmatrix} \leq x_t \leq \begin{bmatrix} i_L^{\max} \\ v_O^{\max} \end{bmatrix} \quad (4.18c)$$

$$u^{\min} \leq u_t \leq u^{\max} \quad (4.18d)$$

$$x_N \in \mathcal{X}_N \quad (4.18e)$$

$$x_0 = x(0) \quad (4.18f)$$

with state and control constraints

$$x^{\min} = \begin{bmatrix} i_L^{\min} \\ v_O^{\min} \end{bmatrix} = \begin{bmatrix} 0 \text{ mA} \\ 0 \text{ V} \end{bmatrix} \quad (4.19)$$

$$x^{\max} = \begin{bmatrix} i_L^{\max} \\ v_O^{\max} \end{bmatrix} = \begin{bmatrix} 200 \text{ mA} \\ 7 \text{ V} \end{bmatrix} \quad (4.20)$$

$$u^{\min} = 0, \quad u^{\max} = 1 \quad (4.21)$$

The matrix weights were $Q = \text{diag}(90, 1)$, $R = 1$, and P was the solution of the

4.5 Learning a faithful still simpler representation of the controller

associated discrete-time algebraic Riccati equation. \mathcal{X}_N was chosen to be the system's maximal invariant set under the corresponding LQR policy. Both the terminal ingredients (P and \mathcal{X}_N) can be easily calculated with the aid of the Multi-Parametric Toolbox (MPT) ? for MATLAB, and are employed to ensure recursive feasibility and closed-loop stability ?.

As a final step, the MPC controller (4.18) was solved off-line using MPT, which yielded a piecewise-affine (PWA) function $\pi(x)$ that maps states directly to optimal control inputs. As well known in the area of explicit model predictive control ?, this function partitions the space of feasible states \mathcal{X} into regions described by sets of linear inequalities. Then, applying the predictive controller on-line boils down to implementing the look-up table of feedback gains

$$u = \pi(x) = \begin{cases} F_1x + g_1, & \text{if } x \in \text{region 1} \\ \dots & \dots \\ F_Mx + g_M, & \text{if } x \in \text{region } M \end{cases} \quad (4.22)$$

As provided by MPT, the computed control policy $\pi(x)$ had $M = 70$ regions, a number too large to be embedded into the target MCU due to the large storage and computational demands (more details are given in Section 4.5). These implementation issues motivate the use of our PWA-NN complexity reduction scheme.

4.5 Learning a faithful still simpler representation of the controller

Explicit MPC controllers are the exact parametric solution of their optimization counterparts. The geometric landscape depicted by the PWA function $\pi(x)$ is composed of numerous linear pieces patched together. At times, neighboring regions share the same control law and, depending on their arrangement, they could be merged into an equivalent single one. Moreover, the overall surface usually presents two scales of complexity: a general shape and, inspecting it more closely, intricate small details. Based on these observations, it is reasonable to try to reproduce the rough shape of $\pi(x)$ without necessarily replicating its small wiggles.

4.5.1 The general architecture

The architecture of the piecewise-affine neural network used to learn $\pi(x)$ is shown in Figure ???. It has two affine layers (L1 and L3), an optimization problem as the activation layer ? (L2) and one projection layer (L4) that in this specific case is simply a saturation function. The latter is needed to ensure that the final control values produced by the NN are within the control bounds $0 \leq u \leq 1$. As discussed in ?, the motivation behind the structure is that of learning the dual MPC problem: L1 maps the state x to the dual space, where L2 represents the dual optimization problem that is solved, L3 then maps the solution back to the primal space, and finally L4 guarantees it respect the control constraints.

As opposed to other approaches to learning MPC controllers with NN ??, the one explored here can be translated to a *closed-form* piecewise-affine function. More specifically, the parametric quadratic program in layer L2 can be solved off-line after training (e.g. by using MPT), yielding a PWA map of the same form as (4.22). The complexity of such function in terms of the number of regions can be adjusted by choosing the size of matrix $H \in \mathbb{R}^{n_z \times n_z}$ inside L2. Fixing n_z also defines the sizes of all remaining trainable parameters highlighted in orange in Figure ???. The result presented next assures the designer that this PWA-NN structure is suitable for any possible predictive controller.

The optimization problem associated with training this NN—in fact, almost any NN architecture—is non-convex. As a consequence, even though there might exist a combination of parameters and weights capable of exactly representing the desired function, reaching them is not an easy task. Since local minima exist, the training process has to be performed multiple times with different initializations. Nevertheless, it is reasonably accepted in the machine learning community that these loss functions possess many high quality local minima, and pursuing a global optimum is irrelevant in this context (see for instance the influential work ?).

Theorem 1 establishes that the size of the NN could be chosen to exactly replicate $\pi(x)$, but that would defeat its purpose since the goal is to learn a faithful but *simpler* version of the MPC controller. For this reason, we gradually increased the size n_z during the training process until a desirable approximation quality was attained. From a machine learning perspective, the problem could be interpreted as an approximation one, where the ground-truth is known.

The explicit control law $\pi(x)$ was sampled in order to collect a set of state-control pairs

$$\{(x_d, u_d) \mid d = 1, \dots, D\} \quad (4.23)$$

4.5 Learning a faithful still simpler representation of the controller

where x_d can be regarded as features and u_d as labels. A total of $D = 5000$ points were gathered randomly using a uniform distribution over the set of feasible states. We highlight that the samples could have been acquired directly from (4.18) as well. Next, the data-points were used to train the internal parameters of the layers shown in Figure ??.

A standard backpropagation approach can be used to iteratively update the NN parameters since, as shown in ?, optimization layers of this type are differentiable (except on sets of measure zero, where subgradients can be used). The PyTorch and OptNet packages for Python were employed to code the NN and mini-batch stochastic gradient descent was used to train it. The batch size was chosen to be 50, and the whole dataset was presented to the algorithm a total of 150 times, i.e., 150 epochs. In order to achieve a balanced learning throughout the domain, the currents and voltages values that formed the input locations x_d were normalized to a range of $[0, 1]$. Furthermore, all trainable weights were initialized randomly. The code was run on a 3.1 GHz Intel Core i7 laptop with 16 GB 2133 MHz of memory. As previously explained, we gradually increased the size n_z of the PWA-NN. Training the network once took approximately 35 mins without any GPU acceleration. With $n_z = 3$, after only 5 initializations, the network presented a very low mean squared error training loss: 1.66×10^{-7} . As for the testing phase, we calculated the true outputs $u = \pi(x)$ and the predicted values $\hat{u} = \hat{\pi}(x)$ on a grid of points; the latter were capable of closely reproducing the original controller as shown in the top plots of Figure ??.

In order to assess the complexity of the learned controller, its L2 layer was converted into a PWA function using the MPT toolbox. As can be seen from lower plots in Figure ??, the number of region was greatly reduced: from 70 in the original partition to 6 in the simplified one, a reduction of 91%. The total memory required to store the control law parameters was reduced from 9.25 kB to 528 B. The latter quantities were calculated by counting the total number of constants needed to describe all the inequalities that compose the polytopes and the remaining NN layers, and assuming that each of them occupies 1 *word* of space.

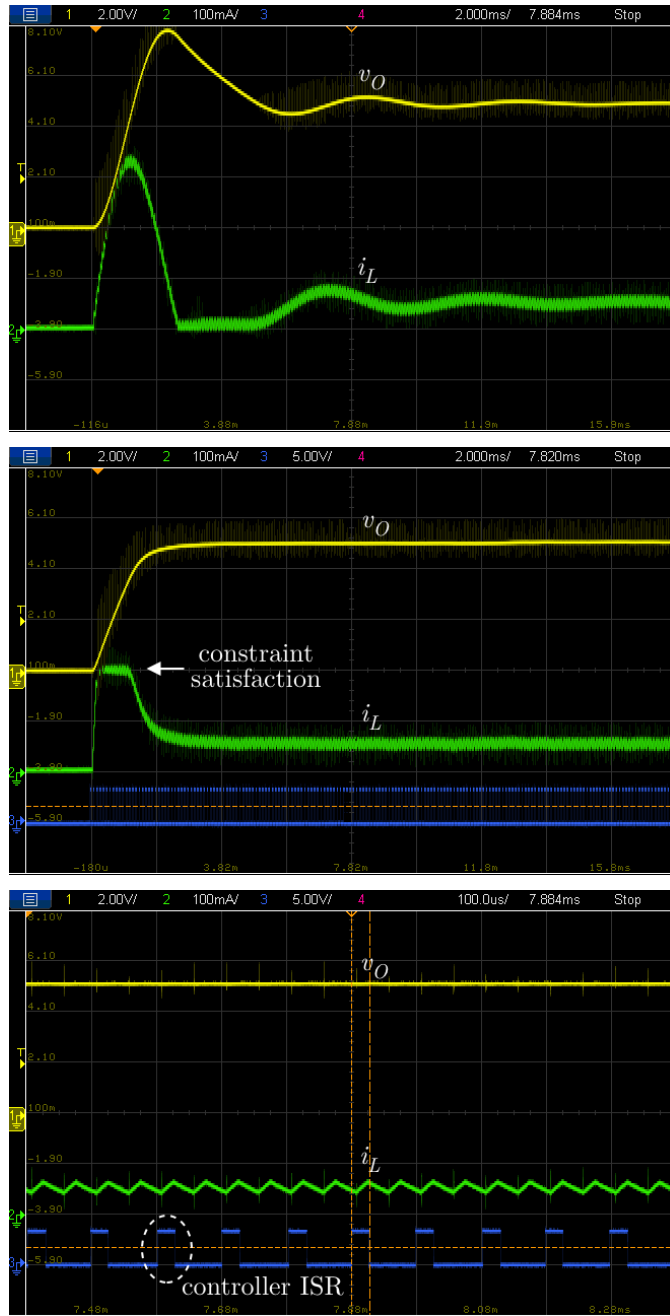


Figure 4.4: Photos of the AHU room depicting the air ducts (top), the supply and return water pipes (top and bottom), and the three-way valve servomotor (bottom).

A Elements of analysis and algebra

For a comprehensive presentation of the concepts, the reader is referred to Searcoid and Searcoid (2002); Pugh (2002).

All vector spaces herein are defined over the field of real numbers \mathbb{R} .

Definition 6. (Metric space) A metric space is a vector space $(V, +, \times)$ equipped with a map $d(\cdot, \cdot) : V \times V \rightarrow \mathbb{R}$ called a *metric* satisfying

$$(i) d(v, v) \geq 0 \quad (\text{A.1})$$

$$(ii) d(v, w) = 0 \Leftrightarrow v = w \quad (\text{A.2})$$

$$(iii) d(v, w) = d(w, v) \quad (\text{A.3})$$

$$(iv) d(v, w) \leq d(v, z) + d(z, w) \quad (\text{A.4})$$

for any $v, w, z \in V$.

For simplicity, we write (V, d) instead of $(V, +, \times, d)$.

Definition 7. (Convergent sequence) Given a metric space (X, d) , a sequence $\{x_n\}_{n \in \mathbb{N}}$ in X is said to *converge* to an element $x \in X$ if

$$\forall \epsilon > 0 : \exists N \in \mathbb{N} : \forall n \geq N : d(x_n, x) < \epsilon \quad (\text{A.5})$$

Convergent sequences are usually written $\lim_{n \rightarrow \infty} x_n = x$ or more simply $x_n \rightarrow x$. Moreover, sequences cannot converge to two or more points.

Definition 8. (Cauchy sequence) Given a metric space (X, d) , a sequence $\{x_n\}_{n \in \mathbb{N}}$ in X is said to be *Cauchy* if

$$\forall \epsilon > 0 : \exists N \in \mathbb{N} : \forall n, m \geq N : d(x_n, x_m) < \epsilon \quad (\text{A.6})$$

Appendix A. Elements of analysis and algebra

Cauchy sequences are a superset of convergent sequences.

Definition 9. (Complete space) A metric space is $(V, +, \times, d)$ is said to be complete if every Cauchy sequence $\{x_n\}_{n \in \mathbb{N}}$ converges to an element $x \in X$.

Definition 10. (Normed space) A normed space is a vector space $(V, +, \times)$ equipped with a map $\|\cdot\| : V \rightarrow \mathbb{R}$ called a *norm* satisfying

$$(i) \|v\| \geq 0 \quad (\text{A.7})$$

$$(ii) \|v\| = 0 \Leftrightarrow v = 0 \quad (\text{A.8})$$

$$(iii) \|\alpha v\| = |\alpha| \|v\| \quad (\text{A.9})$$

$$(iv) \|v + w\| \leq \|v\| + \|w\| \quad (\text{A.10})$$

for any $v, w \in V$ and any $\alpha \in \mathbb{R}$.

Metrics can be defined via norms through $d(x, y) := \|x - y\|$. As a result, every normed space is a metric space.

Definition 11. (Banach space) A normed space $(X, \|\cdot\|)$ is called a Banach space if it is complete.

Definition 12. (Inner-product space) An inner-product space is a vector space $(X, +, \times)$ equipped with a map $\langle \cdot, \cdot \rangle : X \times X \rightarrow \mathbb{R}$ called an *inner-product* satisfying

$$(i) \langle x, y \rangle = \langle y, x \rangle \quad (\text{A.11})$$

$$(ii) \langle \alpha x + \beta y, z \rangle = \alpha \langle x, z \rangle + \beta \langle y, z \rangle \quad (\text{A.12})$$

$$(iii) \langle x, x \rangle \geq 0 \quad (\text{A.13})$$

$$(iv) \langle x, x \rangle = 0 \Leftrightarrow x = 0 \quad (\text{A.14})$$

for any $v, w \in V$ and any $\alpha \in \mathbb{R}$.

Norms can be defined via inner-products through $\|x\| := \sqrt{\langle x, x \rangle}$. As a result, every inner-product space is also a normed space.

Definition 13. (Hilbert space) An inner-product space $(X, \langle \cdot, \cdot \rangle)$ is called a Hilbert space if it is complete.

Definition 14. (Bounded linear operator) Let $(V, \|\cdot\|_V)$ and $(W, \|\cdot\|_W)$ be two Banach spaces. A map $A : V \mapsto W$ is said to be a bounded linear operator if

$$\sup_{v \in V \setminus \{0\}} \frac{\|Av\|_W}{\|v\|_V} < \infty \quad (\text{A.15})$$

Definition 15. (Operator norm) Let $A : V \mapsto W$ be a bounded linear operator. The operator norm is defined as

$$\|A\| := \sup_{v \in V \setminus \{0\}} \frac{\|Av\|_W}{\|v\|_V} \quad (\text{A.16})$$

Definition 16. (Pointwise convergence) Let X, Y be two metric spaces and $\{f_n\}_{n \in \mathbb{N}}$ be a sequence of functions where $f_n : X \rightarrow Y$ for all n . The sequence is said to converge to a function $f : X \rightarrow Y$ if for every $x \in X$

$$\lim_{n \rightarrow \infty} f_n(x) = f(x) \quad (\text{A.17})$$

The example below, taken from (Berlinet and Thomas-Agnan, 2011, §1), highlights an issue one has to pay attention to when working with spaces of functions.

Example 1. (Convergence does not imply pointwise convergence) Let P be the vector space of all polynomials over $[0, 1]$ and endow it with the norm

$$\|f\|_P = \left(\int_0^1 |f(x)|^2 dx \right)^{1/2} \quad (\text{A.18})$$

The sequence $\{p_n\}_{n \in \mathbb{N}}$, $p_n(x) = x^n$ converges to the zero function since

$$\lim_{n \rightarrow \infty} \|p_n - 0\|_P = \lim_{n \rightarrow \infty} \left(\int_0^1 x^{2n} dx \right)^{1/2} \quad (\text{A.19})$$

$$= \lim_{n \rightarrow \infty} \frac{1}{\sqrt{2n+1}} \quad (\text{A.20})$$

$$= 0 \quad (\text{A.21})$$

and yet $p_n(1) = 1, \forall n$, i.e., $|p_n(x) - 0(x)| \not\rightarrow 0$.

Discuss function spaces, convergence and pointwise convergence in them.

B Properties of kernels

Let k , k_1 and k_2 be PD kernels (Definition 3) defined on $\Omega \times \Omega$, $\Omega \subseteq \mathbb{R}^n$. Let $\alpha \geq 0$ be an arbitrary positive scalar. We have that the new function k^* as defined by any of the following constructions is also a PD kernel

$$k^*(x, x') := \alpha k(x, x') \quad (\text{B.1})$$

$$k^*(x, x') := k_1(x, x') + k_2(x, x') \quad (\text{B.2})$$

$$k^*(x, x') := k_1(x, x')k_2(x, x') \quad (\text{B.3})$$

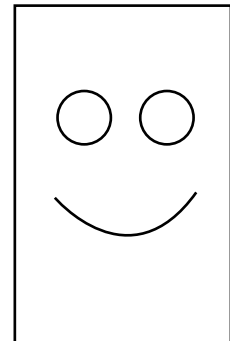
Proof: For the first three cases, see (Steinwart and Christmann, 2008, §4). \square

Bibliography

- Berlinet, A. and Thomas-Agnan, C. (2011). *Reproducing kernel Hilbert spaces in probability and statistics*. Springer Science & Business Media.
- Kidger, P. and Lyons, T. (2020). Universal approximation with deep narrow networks. In *Conference on learning theory*, pages 2306–2327. PMLR.
- Micchelli, C. A., Xu, Y., and Zhang, H. (2006). Universal kernels. *Journal of Machine Learning Research*, 7(12).
- Pugh, C. C. (2002). *Real mathematical analysis*. Springer.
- Schölkopf, B. and Smola, A. J. (2002). *Learning with kernels: support vector machines, regularization, optimization, and beyond*. MIT press.
- Searcoid, M. Ó. and Searcoid, M. (2002). *Elements of abstract analysis*. Springer.
- Sejdinovic, D. and Gretton, A. (2012). What is an RKHS? *Lecture Notes*.
- Steinwart, I. (2020). Reproducing kernel hilbert spaces cannot contain all continuous functions on a compact metric space. *arXiv preprint arXiv:2002.03171*.
- Steinwart, I. and Christmann, A. (2008). *Support vector machines*. Springer Science & Business Media.
- Steinwart, I., Hush, D., and Scovel, C. (2006). An explicit description of the reproducing kernel Hilbert spaces of Gaussian RBF kernels. *IEEE Transactions on Information Theory*, 52(10):4635–4643.
- Temlyakov, V. (2008). Approximation in learning theory. *Constructive Approximation*, 27(1):33–74.
- Wendland, H. (2004). *Scattered data approximation*. Cambridge university press.

Personal details:

| | |
|-------------------------------|--|
| Name : | Mr. Sample CV |
| Address : | Samplestreet 70 6005 Luzern Switzerland |
| Date of Birth : | 2nd of October 1981 |
| Nationality : | Swiss |
| Legally work : | legally work in EU |
| Marital status : | with partner |
| Children : | none |
| | |
| Languages : | Chinese/Mandarin, English, French, German |
| Education level : | Bachelors degree |
| Hospitality work experience : | 3-5 years |
| Special experience : | Europe work experience |
| | |
| Date of availability : | September 2009 |
| Current location : | Africa |
| Travelling Status : | will be travelling single status |
| Telephone : | 0041 41 370 6759 |
| Email address : | jeff@h-g-r.com |
| Position(s) sought : | Permanent position for graduates |
| Department(s) sought : | Food & Beverage Bar/Sommelier |



Personal profile:

As a Bachelor of Business Administration and after obtaining first relevant international work experience within the hospitality industry, I am now ready to take on new responsibilities to further my professional career. My key strengths include strong analytical and logical skills, an eye for detail, communication and interpersonal skills. I enjoy working in a team and help others progress. At the same time I work well independently. As a highly motivated and driven individual I strive on taking up challenges.

Interests:

Travelling
Foreign Cultures
Photography
Sports

Educational qualifications:

| | |
|-----------------|-----------------------------------|
| Oct 99 - Feb 02 | Higher Diploma (Hotel Management) |
| | Swiss Hotelmanagement School, SHL |

Employment history:

| | |
|------------------|--|
| Mar 04 - Ongoing | Assistant Manager (Rooms Division/Food & Beverage) Hotel Atlantic Kempinski Hamburg www.kempinski.com 5 star business hotel, part of Leading Hotels of the World 412 guest rooms, large function facilities, 3 food & beverage outlets Optimization of bar procedures, reinforcing SOPs Developing & implementing promotions Responsible for day-to-day operations Optimization and streamlining of housekeeping and laundry procedures Implementation of new SOPs Analyzing monthly reports for rooms division performance and sub departments |
| Mar 03 - Mar 04 | Management Trainee Hospitality Graduate Recruitment www.h-g-r.com Leading company for placements within the Hospitality industry. Traineeship covering all aspects of an online recruitment agency. |
| Mar 02 - Mar 03 | Management Trainee (Rooms Division) Hyatt Regency Xian, China www.hyatt.com 5 star business hotel 404 guest rooms, 4 food & beverage outlets Traineeship covering all rooms division departments on operational as well as supervisory level. |

Training courses attended:

| | |
|------------------|---------------------------|
| Mar 02 - Ongoing | OpenOffice - IT Courses |
| May 01 - Jan 03 | Language Course - Chinese |

References:

Hyatt Regency Xian
Patrick Sawiri, Phone: 86 22 2330 7654

Hospitality Graduate Recruitment
Jeff Ross, Phone: 41 41 370 99 88